

Dynamic Factor Analysis with Dependent Gaussian Processes for High-Dimensional Gene Expression Trajectories

Jiachen Cai, Robert J. B. Goudie, Colin Starr, Brian D. M. Tom¹

¹MRC Biostatistics Unit, University of Cambridge, UK

Abstract

The increasing availability of high-dimensional, longitudinal measures of genetic expression can facilitate analysis of the biological mechanisms of disease and prediction of future trajectories, as required for precision medicine. Biological knowledge suggests that it may be best to describe complex diseases at the level of underlying pathways, which may interact with one another. We propose a Bayesian approach that allows for characterising such correlation among different pathways through Dependent Gaussian Processes (DGP) and mapping the observed high-dimensional gene expression trajectories into unobserved low-dimensional pathway expression trajectories via Bayesian Sparse Factor Analysis. Compared to previous approaches that model each pathway expression trajectory independently, our model demonstrates better performance in recovering the shape of pathway expression trajectories, revealing the relationships between genes and pathways, and predicting gene expressions (closer point estimates and narrower predictive intervals), as demonstrated in the simulation study and real data analysis. To fit the model, we propose a Monte Carlo Expectation Maximization (MCEM) scheme that can be implemented conveniently by combining a standard Markov Chain Monte Carlo sampler and an R package GPFDA (Konzen et al., 2021), which returns the maximum likelihood estimates of DGP parameters. The modular structure of MCEM makes it generalizable to other complex models involving the DGP model component. An R package has been developed that implements the proposed approach.

Keywords: High-Dimensional Gene Expression Trajectories; Multivariate Longitudinal Data; Pathways; Sparse Factor Analysis; Dependent Gaussian Processes; Monte Carlo Expectation Maximization.

1 Introduction

The development of high-throughput technology has enabled researchers to collect high-dimensional genomic data repeatedly over time, facilitating the discovery of disease mechanisms. Biological knowledge suggests that it may be best to describe complex diseases at the level of pathways, rather than

the level of individual genes (Richardson et al., 2016). A biological pathway is a series of interactions among molecules that results in a certain biological function or response or describe a particular mechanism or phenomena. Pathways are sometimes summarized by activity scores derived from genes expression values (Temate-Tiagueu et al., 2016) with corresponding gene set; such scores form a basis of making comparisons between people in different clinical statuses (Vaske et al., 2010; Wang et al., 2019; Kim et al., 2021). The relationship between genes and pathways can be illustrated (in a simplified representation) using Figure 1. Each pathway involves only a small proportion of genes (sparsity), where some genes may not contribute to any relevant pathway (e.g. gene 4), may contribute to a single pathway (e.g. gene 1 only contributes to pathway 1 and gene 3 only contributes to pathway 2), or may contribute to multiple pathways (e.g. gene 2 contributes to both pathways). Pathways are often unobservable in practice. Therefore, recovering their trajectories from observed gene expression data has been one of the major interests in genomic data analysis.

The Bayesian Sparse Factor Analysis (BSFA) model is an established statistical approach used to map high-dimensional gene expression data to a low-dimensional pathway expression representation; the former are treated as observed variables and the latter as latent factors (Carvalho et al., 2008; Chen et al., 2011). One of the main assumptions in BSFA is the independence of factors. In our context, this assumption means that the expressions of pathways are uncorrelated. However, this may not be true biologically. In fact, previous research has found that pathways often interact with one another to achieve complex biological functions (Hsu and Yang, 2012).

In this paper we propose relaxing the classical assumption of independent factors to allow for the possibility of correlated factors, and estimate the cross-correlation among the factors from data. To do this, we model the latent factor trajectories using Dependent Gaussian Processes (DGP). As we will show in the simulation study and real data analysis, our approach performs better at recovering the shape of latent factor trajectories, estimating the relationship between genes and pathways, and predicting future gene expression.

In addition to the modeling innovation, another contribution of this paper is with regard to the algorithm developed for estimating parameters of the DGP model when it is embedded within another model. To obtain the maximum likelihood estimate (MLE) of the DGP parameters, we developed a Monte Carlo Expectation Maximization (MCEM) algorithm, which can be conveniently implemented by combining an existing R package, GPFDA (Konzen et al., 2021), with a standard Markov Chain Monte Carlo (MCMC) sampler. An R package DGP4LCF (Dependent Gaussian Processes for Longitudinal Correlated Factors) has been developed to implement the proposed method; available on Github: <https://github.com/jcai-1122/DGP4LCF>.

The remainder of the article is organized as follows. In Section 2, we review BSFA and DGP, then

propose our integrated model based on them. In Section 3, we introduce the inference method for the proposed model, and discuss identifiability issues with the model and our approach to addressing these. We explore various aspects of the behavior of our proposed approach under different factor generation mechanisms in the simulation study in Section 4: prediction of gene expression, estimation of gene-pathway relationships and the shape of pathway expression trajectories; and we demonstrate that its performance in the aforementioned aspects is always superior to the traditional model ignoring correlation among factors. In Section 5, we apply the proposed method to real data and compare our results with a previous analysis in Chen et al. (2011). We conclude with a discussion on future research directions in Section 6.

2 Model

Let t_{ij} denote the j th measured time point of the i th individual, $i = 1, \dots, n$, $j = 1, \dots, q_i$, where n and q_i are the number of subjects and subject-specific time points, respectively. At time t_{ij} , x_{ijg} is the g th gene expression, $g = 1, \dots, p$, where p is the number of genes. We seek to describe these data in terms of k latent factors/pathways y_{ija} , $a = 1, \dots, k$. In practice, we expect k to be much smaller than p .

Throughout this paper we assume that k is pre-specified and fixed, with the choice primarily based on previous knowledge about the data at hand. Note, however, that it may be possible to identify when k is unnecessarily large (as we will show in the simulation study), since redundant factors will have no significantly loaded genes.

Our proposed model is based on BSFA and DGP. Therefore, before presenting the proposed model in Section 2.3, we first introduce BSFA in Section 2.1 and DGP in Section 2.2.

2.1 Uncovering Sparse Factor Structure via BSFA

The BSFA model connects observations x_{ijg} with the unobserved latent factors y_{ija} via a factor loading matrix $\mathbf{L} = \{l_{ga}\}_{g=1, \dots, p, a=1, \dots, k} \in \mathbb{R}^{p \times k}$, and incorporates the prior belief of sparsity by imposing a sparsity-inducing prior distribution on \mathbf{L} . It can be expressed as follows,

$$x_{ijg} = \mu_{ig} + \sum_{a=1}^k l_{ga} y_{ija} + e_{ijg}, \quad (1)$$

where μ_{ig} is the intercept term for the g th gene of the i th individual (hereafter the “subject-gene mean”), e_{ijg} is the residual error, and each element l_{ga} quantifies the extent to which the g th gene expression is related to the a th pathway expression, with larger absolute values indicating a stronger

contribution of the gene expression to the pathway expression. In this paper, we assume l_{ga} is constant across all time points.

We adopt point-mass mixture priors to induce sparsity (Bernardo et al., 2003; Carvalho et al., 2008) because we want the model to shrink insignificant parameters completely to zero, without the need to further set up a threshold for inclusion, as in continuous shrinkage priors (Bhattacharya and Dunson, 2011). The point-mass mixture prior is introduced by first decomposing l_{ga} as the product of a binary variable Z_{ga} indicating inclusion and a continuous variable A_{ga} denoting the regression coefficient, and then specifying a Bernoulli-Beta prior for Z_{ga} and a Normal-Inverse-Gamma prior for A_{ga} :

$$\begin{aligned} l_{ga} &= Z_{ga} \cdot A_{ga}, \\ Z_{ga} &\sim \text{Bern}(\pi_a), \pi_a \sim \text{Beta}(c_0, d_0), \\ A_{ga} &\sim \text{N}(0, \rho_a^2), \rho_a^2 \sim \text{Inverse-Gamma}(c_1, d_1), \end{aligned} \tag{2}$$

where $g = 1, \dots, p; a = 1, \dots, k$ and c_0, d_0, c_1, d_1 are pre-specified positive constants. An *a priori* belief about sparsity can be represented via (c_0, d_0) , which controls the proportion of genes π_a that contributes to the a th pathway. If $Z_{ga} = 0$, meaning that the g th gene does not contribute to the a th pathway, then the corresponding loading $l_{ga} = 0$; otherwise the loading is drawn from the prior distribution $\text{N}(0, \rho_a^2)$.

We complete the model specification by assigning a Normal-Inverse-Gamma prior to both subject-gene means μ_{ig} and residuals e_{ijg} ,

$$\begin{aligned} \mu_{ig} &\sim \text{N}(\mu_g, \sigma_g^2), & \sigma_g^2 &\sim \text{Inverse-Gamma}(c_2, d_2), \\ e_{ijg} &\sim \text{N}(0, \phi_g^2), & \phi_g^2 &\sim \text{Inverse-Gamma}(c_3, d_3), \end{aligned}$$

where μ_g is fixed as the mean of the g th gene expression across all time points of all people, and c_2, d_2, c_3, d_3 are pre-specified positive constants.

To implement the BSFA model, the software BFRM has been developed (Carvalho et al., 2008). However, the current version of BFRM has two major limitations. First, it only returns point estimates of parameters, without any quantification of uncertainty. Second, it can handle only independent data; therefore it does not account for within-individual correlation when supplied with longitudinal data.

2.2 Modeling Correlated, Time-Dependent Factor Trajectories via DGP

Several approaches treating factor trajectories $y_a(t)$, $a = 1, \dots, k$ as functional data have been proposed, including spline functions (Ramsay et al., 2009), differential equations (Ramsay and Hooker, 2019), autoregressive models (Penny and Roberts, 2002), and Gaussian Processes (GP) (Shi and Choi, 2011). As mentioned previously, we are interested in incorporating the cross-correlation among different factors into the model. GPs are well-suited to this task because DGPs can account for the interdependence of factors in a straight-forward manner. Indeed, the DGP model has been widely applied to model dependent multi-output time series in the machine learning community (Alvarez and Lawrence, 2011), where it is also known as “multitask learning”. Sharing information between tasks using DGPs can improve prediction compared to using Independent Gaussian Processes (IGPs) (Caruana, 1997; Bonilla et al., 2007). DGPs have also been used to model correlated, multivariate spatial data in the field of geostatistics (Genton and Kleiber, 2015), improving prediction performance over IGPs (Dey et al., 2020).

The main difficulty with DGP modeling is how to appropriately define cross-covariance functions that imply a positive definite covariance matrix. Liu et al. (2018) reviewed existing strategies developed to address this issue and found, in simulation studies, that no single approach outperformed all others in all scenarios. When the intent was to improve the predictions of all the outputs jointly (such is our case here), the kernel convolution framework (KCF) (Boyle and Frean, 2005a) was among the best performers. The KCF has also been widely employed by other researchers (Alvarez and Lawrence, 2011; Shi et al., 2017). Therefore, we adopt the KCF strategy for DGP modeling here, and a detailed illustration can be found in Section A.2. of the supplementary materials.

The distribution of $(y_{i1a}, \dots, y_{iq_ia}, y_{i1b}, \dots, y_{iq_ib})^T$ induced under KCF is a multivariate normal distribution (MVN) with mean vector $\mathbf{0}$ and covariance matrix fully determined by parameters of kernel functions and the noise parameter; we will use Θ to denote all of them hereafter. The covariance matrix contains the information of both the auto-correlation for each single process and the cross-correlation between different processes. In this paper, we focus on the cross-correlation, which correspond to interactions across different biological pathways that have been ignored in previous analysis (Chen et al., 2011).

The KCF can be implemented via the R package GPFDA (Konzen et al., 2021), which outputs the MLE for DGP parameters given measurements of the processes $y_a(t)$, $a = 1, \dots, k$. Its availability inspired and facilitated the algorithm developed for the proposed model. GPFDA assumes all input processes are measured at common time points, which is often unrealistic in practice; but we will show the adaptation of GPFDA to our case of subject-specific time points in Section 3.

2.3 Proposed Integrated Model

We propose a model that combines BSFA and DGP (referred as “BSFA-DGP” hereafter), and present it in matrix notation below. To accommodate irregularly measured time points across individuals, we first introduce the vector of all unique observation times $\mathbf{t} = \bigcup_{i=1}^n \mathbf{t}_i$ across all individuals, and denote its length as q ; each $\mathbf{t}_i = \bigcup_{j=1}^{q_i} t_{ij}$ is a vector of observed time points for the i th individual. Let $\mathbf{Y}_i = (\mathbf{y}_{i1}, \dots, \mathbf{y}_{ik})^T \in \mathbb{R}^{k \times q}$ be the matrix of pathway expression, with $\mathbf{y}_{ia} = (y_{i1a}, \dots, y_{iqa})^T$ denoting the a th factor’s expression across all observation times \mathbf{t} ; and let $\mathbf{Y}_{i,\text{obs}}, \mathbf{Y}_{i,\text{miss}}$ be the sub-matrices of \mathbf{Y}_i , denoting pathway expression at times when gene expression of the i th person are observed and missing, respectively. Let $\text{vec}(\mathbf{Y}_i^T)$ denote the column vector obtained by stacking the columns of matrix \mathbf{Y}_i^T on top of one another; similar definitions apply to $\text{vec}(\mathbf{Y}_{i,\text{obs}}^T)$ and $\text{vec}(\mathbf{Y}_{i,\text{miss}}^T)$.

Let $\mathbf{X}_i = (\mathbf{x}_{i1}, \dots, \mathbf{x}_{ip})^T \in \mathbb{R}^{p \times q_i}$ be the matrix of gene expression measurements at the q_i observation times for the i th individual, with $\mathbf{x}_{ig} = (x_{i1g}, \dots, x_{iq_i g})^T$ denoting the g th gene’s trajectory; and correspondingly let $\mathbf{M}_i = (\boldsymbol{\mu}_{i1}, \dots, \boldsymbol{\mu}_{ip})^T \in \mathbb{R}^{p \times q_i}$ be the matrix of subject-gene means, with $\boldsymbol{\mu}_{ig} = \mu_{ig} \mathbf{1}$, where $\mathbf{1}$ is a q_i -dimensional column vector consisting of the scalar 1. Furthermore, let $\mathbf{A} = \{A_{ga}\}_{g=1, \dots, p; a=1, \dots, k} \in \mathbb{R}^{p \times k}$ be the matrix of regression coefficients and $\mathbf{Z} = \{Z_{ga}\}_{g=1, \dots, p; a=1, \dots, k} \in \mathbb{R}^{p \times k}$ be the matrix of inclusion indicators,

$$\begin{aligned} \mathbf{X}_i &= \mathbf{M}_i + \mathbf{L}\mathbf{Y}_{i,\text{obs}} + \mathbf{E}_i, \\ \mathbf{L} &= \mathbf{A} \circ \mathbf{Z}, \\ \text{vec}(\mathbf{Y}_i^T) &\sim \text{MVN}(\mathbf{0}, \Sigma_{\mathbf{Y}}) \end{aligned} \tag{3}$$

where \circ denotes element-wise matrix multiplication, $\Sigma_{\mathbf{Y}} \in \mathbb{R}^{kq \times kq}$ is the covariance matrix induced via the KCF modeling, and \mathbf{E}_i is the residual matrix. The prior distributions for components of \mathbf{A} , \mathbf{Z} , \mathbf{M}_i , and \mathbf{E}_i have been described in Section 2.1.

3 Inference

In this section, we describe inference for our proposed model. We develop an MCEM framework to obtain the MLE for DGP parameters $\boldsymbol{\Theta}$ in Section 3.1 and the framework is summarized in Algorithm 1. For fixed DGP parameter values, we propose a Gibbs sampler for the other variables in the model, denoted by $\boldsymbol{\Omega} = \{\mathbf{M}, \mathbf{Y}, \mathbf{A}, \mathbf{Z}, \boldsymbol{\rho}, \boldsymbol{\pi}, \boldsymbol{\sigma}, \boldsymbol{\phi}\}$, where $\mathbf{M} = \{\mathbf{M}_i\}_{i=1, \dots, n}$, $\mathbf{Y} = \{\mathbf{Y}_i\}_{i=1, \dots, n}$, $\boldsymbol{\rho} = \{\rho_a^2\}_{a=1, \dots, k}$, $\boldsymbol{\pi} = \{\pi_a\}_{a=1, \dots, k}$, $\boldsymbol{\sigma} = \{\sigma_g^2\}_{g=1, \dots, p}$, $\boldsymbol{\phi} = \{\phi_g^2\}_{g=1, \dots, p}$ (Section 3.2). This sampler serves two purposes. First, within the MCEM algorithm (called “Gibbs-within-MCEM” hereafter), it generates samples for approximating the expectation in Equation 7, which is used for updating estimates of $\boldsymbol{\Theta}$. Second, after

the final DGP estimate, denoted by $\hat{\Theta}^{\text{MLE}}$, is obtained from MCEM, we proceed with implementing the sampler (called “Gibbs-after-MCEM” hereafter and a summary is provided in Supplementary Algorithm 1) to find the final posterior distribution of interest, which is $f(\Omega|\mathbf{X}, \hat{\Theta}_{\text{MLE}})$, where $\mathbf{X} = \{\mathbf{X}_i\}_{i=1,\dots,n}$ represents observed gene expression. Finally, we discuss the underlying reason for and our approach to addressing the identifiability issues encountered throughout the whole process of inference in Section 3.3.

3.1 MCEM Framework for Estimating Cross-Correlation Determined by DGP Parameters

3.1.1 Options for Estimating DGP Parameters

To estimate the DGP parameters Θ , two strategies have been widely adopted: Fully Bayesian (FB) and Empirical Bayesian (EB). The former proceeds by assigning prior distributions to Θ to account for our uncertainty. The latter proceeds by fixing Θ to reasonable values based on the data; for example, we can set them to the MLE. Compared to FB, EB sacrifices the quantification of uncertainty for a lower computational cost. Here, we adopt the EB approach because the key quantities of interest for inference in our model are the factor loading matrix \mathbf{L} , latent factors \mathbf{Y}_i , and the prediction of gene expression, rather than DGP parameters Θ . Therefore, we simply want a reasonably good estimate of Θ to proceed, without expending excessive computation time.

3.1.2 Finding the MLE for DGP Parameters via an MCEM Framework

To derive $\hat{\Theta}^{\text{MLE}}$, we first write out the marginal likelihood function with respect to Θ for our proposed model in Section 2.3, with f denoting probability density function,

$$\begin{aligned} f(\mathbf{X}|\Theta) &= \int f(\mathbf{X}, \Omega|\Theta) d\Omega \\ &= \int f(\mathbf{X}|\mathbf{M}, \mathbf{Y}, \mathbf{A}, \mathbf{Z}, \phi) f(\mathbf{M}|\sigma) f(\mathbf{Y}|\Theta) f(\mathbf{A}|\rho) f(\mathbf{Z}|\pi) f(\phi) f(\sigma) f(\rho) f(\pi) d\Omega, \end{aligned} \quad (4)$$

which requires high-dimensional integration.

To deal with the integration, one strategy is the Expectation-Maximization (EM) algorithm (Dempster et al., 1977). Here, we view Ω as the hidden variables, and Θ as the parameters to be estimated by maximum likelihood. The essential idea of EM is to iteratively construct a series of estimates $\hat{\Theta}^{(l)}$, $l = 1, 2, 3, \dots$, that converges to $\hat{\Theta}^{\text{MLE}}$ (Wu, 1983). Specifically, each iteration involves two alternating steps. Assuming the algorithm is at its l th iteration, the first step requires evaluation of the conditional expectation of the log-likelihood of the complete data $\{\mathbf{X}, \Omega\}$ given the observed data \mathbf{X} and the previously iterated parameter value $\hat{\Theta}^{(l-1)}$. This step is known as the expectation step (E-Step),

and the conditional expectation is called the “Q-function”,

$$Q(\Theta, \hat{\Theta}^{(l-1)}) = \mathbb{E}_{\Omega} \left[\ln f(\mathbf{X}, \Omega | \Theta) \mid \mathbf{X}, \hat{\Theta}^{(l-1)} \right]. \quad (5)$$

In the second step, this expectation is maximized to obtain the updated parameter $\hat{\Theta}^{(l)}$,

$$\hat{\Theta}^{(l)} = \arg \max_{\Theta} Q(\Theta, \hat{\Theta}^{(l-1)}). \quad (6)$$

Therefore, this step is known as the maximization step (M-Step). The EM algorithm keeps updating parameters in this way until the pre-specified stopping condition is met.

As for many complex models, the analytic form of the aforementioned conditional expectation in Equation 5 is unavailable. To address this issue, a Monte Carlo version of EM (MCEM) has been developed (Wei and Tanner, 1990; Levine and Casella, 2001; Casella, 2001), which uses Monte Carlo samples to approximate the exact expectation. Casella (2001) showed that MCEM has attractive statistical properties: it is able to result in consistent estimates of posterior distributions and asymptotically valid confidence sets. MCEM has been widely applied before in different models (Havasi et al., 2018; Guan and Haran, 2019; Molstad et al., 2021); but to the best of our knowledge, this paper is the first use of MCEM in the context of the DGP model.

Suppose that we have R samples $\{\Omega^r\}_{r=1, \dots, R}$ drawn from the posterior distribution $f(\Omega | \mathbf{X}, \hat{\Theta}^{(l-1)})$ using an MCMC sampler (details of the sampler are provided in Section 3.2), then Equation 5 can be approximated as,

$$Q(\Theta, \hat{\Theta}^{(l-1)}) \approx \tilde{Q}(\Theta, \hat{\Theta}^{(l-1)}) = \frac{1}{R} \sum_{r=1}^R \ln f(\mathbf{X}, \Omega^r | \Theta). \quad (7)$$

Similar to Equation 4, the complete data likelihood $f(\mathbf{X}, \Omega^r | \Theta)$ can be decomposed as,

$$\begin{aligned} f(\mathbf{X}, \Omega^r | \Theta) &= f(\mathbf{X} | \mathbf{M}^r, \mathbf{Y}^r, \mathbf{A}^r, \mathbf{Z}^r, \phi^r) \cdot f(\mathbf{M}^r | \sigma^r) \cdot f(\mathbf{Y}^r | \Theta) \cdot \\ & f(\mathbf{A}^r | \rho^r) \cdot f(\mathbf{Z}^r | \pi^r) \cdot f(\phi^r) \cdot f(\sigma^r) \cdot f(\rho^r) \cdot f(\pi^r). \end{aligned} \quad (8)$$

The M-Step maximizes Equation 7 with respect to Θ , and from Equation 8 the only term that depends on Θ is $f(\mathbf{Y}^r | \Theta)$. Therefore, the approximated Q-function in Equation 7 can be simplified as,

$$\tilde{Q}(\Theta, \hat{\Theta}^{(l-1)}) = \frac{1}{R} \sum_{r=1}^R \ln f(\mathbf{Y}^r | \Theta). \quad (9)$$

This simplification implies that, the maximizer $\hat{\Theta}^{(l)}$ for Equation 7 is exactly the same as that of Equation 9. As a result, the task has now been reduced to finding Θ that can maximize the likelihood function of $\{\mathbf{Y}^r\}_{r=1,\dots,R} = \{\mathbf{Y}_i^r\}_{i=1,\dots,n;r=1,\dots,R}$, given that each \mathbf{Y}_i^r follows a DGP distribution determined by Θ . Although gene expressions are measured at irregular time points for different individuals, samples of latent factors are available at common times \mathbf{t} ; therefore enabling the use of GPFDA to estimate the MLE.

The MCEM framework described above is summarized in Algorithm 1. Its implementation challenges are rooted in one common consideration: the computational cost of the algorithm. We discuss these challenges, including the choice of MCMC sample size R and the stopping condition, in Section 3.1.3 and 3.1.4, respectively.

3.1.3 Choosing MCMC Sample Size

First and foremost, the Gibbs-within-MCEM sample size R determines the computational cost for both the Gibbs sampler and EM. Choosing R too small, while saving computational expense for the Gibbs sampler, results in a less precise approximation of the Q-function, and thus leads to significantly slower convergence of the EM algorithm. In contrast, choosing R too large, while providing an accurate approximation of the Q-function and faster EM convergence, results in the time taken for generating the required Gibbs samples becoming prohibitive. Consequently, the choice of R must trade-off the accuracy of the Q-function with the computational cost of generating Gibbs-within-MCEM samples. We provided a literature review on this topic in Section A.3.1. of the supplementary materials and adapted the approach proposed by Caffo et al. (2005) to our model, which automatically determines when to increase R dependent on whether the ascent property of the marginal likelihood under EM is preserved or not (Wu, 1983). Section A.3.2. shows the derivation of the adapted algorithm.

3.1.4 Specifying the Stopping Condition

The other challenge when implementing the MCEM algorithm is to specify the stopping criterion. This can be based on the change in individual parameter estimates (Booth and Hobert, 1999), the marginal likelihood (Newton and Raftery, 1994), or the Q-function (Caffo et al., 2005). If there is little change between consecutive values, then the algorithm can be stopped. We propose to stop the algorithm when the total number of sample size increase exceeds a pre-specified value W ; by doing so, the number of Gibbs samples and samples input to GPFDA is bounded, therefore ensuring the MCEM algorithm can return results within reasonable time.

Finally, post-processing Gibbs samples $\{\mathbf{Y}^r\}_{r=1,\dots,R}$ (including burn-in and thinning) before inputting them to GPFDA can help drastically reduce the computational cost of GPFDA while still

preserving most information in the samples.

3.2 Gibbs Sampler for Other Variables under Fixed GP Estimates

To acquire samples for $\mathbf{\Omega}$ from the posterior distribution under fixed DGP estimates $f(\mathbf{\Omega}|\mathbf{X}, \hat{\mathbf{\Theta}})$, we use a Gibbs sampler since the full conditionals for all variables in $\mathbf{\Omega}$ are analytically available. We summarise the high-level approach here; the details of the full conditionals are available in Section A.1. of the supplementary materials.

For the key variables \mathbf{Z} , \mathbf{A} , and \mathbf{Y} , we use blocked Gibbs to improve mixing. To block-update the g th row of the binary matrix \mathbf{Z} , we compute the posterior probability under 2^k possible values of (Z_{g1}, \dots, Z_{gk}) , then sample with corresponding probabilities. To update the g th row of the regression coefficient matrix \mathbf{A} , (A_{g1}, \dots, A_{gk}) , we draw from a MVN distribution.

When updating $\text{vec}(\mathbf{Y}_i^T)$, the vectorized form of the i th individual's factor scores, we divide it into two groups $\text{vec}(\mathbf{Y}_i^T) = (\text{vec}(\mathbf{Y}_{i,\text{obs}}^T), \text{vec}(\mathbf{Y}_{i,\text{miss}}^T))$ because the form of the conditional posterior distributions differ. We first sample $\text{vec}(\mathbf{Y}_{i,\text{obs}}^T)$ and then $\text{vec}(\mathbf{Y}_{i,\text{miss}}^T)$,

$$f(\text{vec}(\mathbf{Y}_i^T)|\mathbf{X}, \hat{\mathbf{\Theta}}, \mathbf{\Omega} \setminus \text{vec}(\mathbf{Y}_i^T)) = f(\text{vec}(\mathbf{Y}_{i,\text{obs}}^T)|\mathbf{X}_i, \hat{\mathbf{\Theta}}, \mathbf{\Omega} \setminus \text{vec}(\mathbf{Y}_i^T)) \cdot f(\text{vec}(\mathbf{Y}_{i,\text{miss}}^T)|\text{vec}(\mathbf{Y}_{i,\text{obs}}^T), \hat{\mathbf{\Theta}}),$$

where $\mathbf{\Omega} \setminus \text{vec}(\mathbf{Y}_i^T)$ denotes the remaining parameters excluding $\text{vec}(\mathbf{Y}_i^T)$. The first term follows a MVN distribution depending on measured gene expression, and the second term also follows a MVN distribution according to standard properties of the DGP model (Shi and Choi, 2011).

3.3 Identifiability Issue of the Proposed Model

To facilitate illustrating the identifiability issue, we first re-express the proposed model in Section 2.3 as,

$$\begin{aligned} \text{vec}(\mathbf{X}_i^T) &= \text{vec}(\mathbf{M}_i^T) + \mathbf{L}_i^* \text{vec}(\mathbf{Y}_{i,\text{obs}}^T) + \text{vec}(\mathbf{E}_i^T), \\ \text{vec}(\mathbf{Y}_i^T) &\sim \text{MVN}(\mathbf{0}, \Sigma_{\mathbf{Y}}), \\ \text{vec}(\mathbf{E}_i^T) &\sim \text{MVN}(\mathbf{0}, \Sigma_{\mathbf{X}_i}), \end{aligned} \tag{10}$$

where $\text{vec}(\mathbf{X}_i^T)$, $\text{vec}(\mathbf{M}_i^T)$, and $\text{vec}(\mathbf{E}_i^T)$ are vectorized from matrices \mathbf{X}_i^T , \mathbf{M}_i^T , and \mathbf{E}_i^T , respectively. To make the above equations hold, \mathbf{L}_i^* and $\Sigma_{\mathbf{X}_i}$ are constructed using components of \mathbf{L} and ϕ , respectively. Specific forms are available in Section A.1. of the supplementary materials.

The distribution of $\text{vec}(\mathbf{X}_i^T)$ after integrating out $\text{vec}(\mathbf{Y}_{i,\text{obs}}^T)$, is

$$\text{vec}(\mathbf{X}_i^T) \mid \text{vec}(\mathbf{M}_i^T), \mathbf{L}_i^*, \Sigma_{\mathbf{X}_i}, \Sigma_{\mathbf{Y}} \sim \text{MVN}(\text{vec}(\mathbf{M}_i^T), \mathbf{L}_i^* \Sigma_{\mathbf{Y}_{i,\text{obs}}} (\mathbf{L}_i^*)^T + \Sigma_{\mathbf{X}_i}), \quad (11)$$

where $\Sigma_{\mathbf{Y}_{i,\text{obs}}}$ is a sub-matrix of $\Sigma_{\mathbf{Y}}$ that characterizes the covariance structure for $\text{vec}(\mathbf{Y}_{i,\text{obs}}^T)$.

The identifiability issue arises from the invariance of the covariance $\mathbf{L}_i^* \Sigma_{\mathbf{Y}_{i,\text{obs}}} (\mathbf{L}_i^*)^T + \Sigma_{\mathbf{X}_i}$ in Equation 11. The uniqueness of $\Sigma_{\mathbf{X}_i}$ has been ensured in previous research (Ledermann, 1937; Bekker and ten Berge, 1997; Conti et al., 2014; Papastamoulis and Ntzoufras, 2022); given its identifiability, we are concerned with identifiability of the factor loadings \mathbf{L}_i^* , the factor scores $\text{vec}(\mathbf{Y}_{i,\text{obs}}^T)$ and $\Sigma_{\mathbf{Y}_{i,\text{obs}}}$. Non-identifiability is present because for any non-singular transformation matrix $\mathbf{D} \in \mathbb{R}^{k_{q_i} \times k_{q_i}}$, the covariances of the estimator $\{\widehat{\mathbf{L}}_i^*, \widehat{\text{vec}(\mathbf{Y}_{i,\text{obs}}^T)}, \widehat{\Sigma}_{\mathbf{Y}_{i,\text{obs}}}\}$ and the transformed estimator $\{\widehat{\mathbf{L}}_i^* \mathbf{D}, \mathbf{D}^{-1} \widehat{\text{vec}(\mathbf{Y}_{i,\text{obs}}^T)}, \mathbf{D}^{-1} \widehat{\Sigma}_{\mathbf{Y}_{i,\text{obs}}} (\mathbf{D}^{-1})^T\}$ are equal. To address the issue, we first place a constraint on $\Sigma_{\mathbf{Y}}$ that requires its diagonal element to be 1. In other words, the covariance matrix of latent factors $\Sigma_{\mathbf{Y}}$ was forced to be a correlation matrix. This restriction ensures the uniqueness of $\Sigma_{\mathbf{Y}}$, and has also been used in Conti et al. (2014).

However, under particular classes of transformation matrices, $\{\mathbf{L}_i^*, \text{vec}(\mathbf{Y}_{i,\text{obs}}^T)\}$ are still not identifiable. This is because $\mathbf{D}^{-1} \widehat{\Sigma}_{\mathbf{Y}_{i,\text{obs}}} (\mathbf{D}^{-1})^T$ might still equal $\widehat{\Sigma}_{\mathbf{Y}_{i,\text{obs}}}$ when \mathbf{D} is a specific signed matrix (diagonal matrix with diagonal elements being 1 or -1) or permutation matrix (under this case, the identifiability problem is also known as *label switching*). The specific form of the transformation matrix leading to such invariance depends on the real correlation structure of the data. To deal with this unidentifiability, we use the R package “factor.switch” developed by Papastamoulis and Ntzoufras (2022) to align samples across Gibbs iterations. Alignment of $\{\mathbf{L}^r, \mathbf{Y}^r\}_{r=1,\dots,R}$ should be completed before inputting factor scores to GPFDA for estimating DGP parameters Θ within the MCEM algorithm, and also before the final posterior summary of $\{\mathbf{L}, \mathbf{Y}\}$ using the Gibbs-After-MCEM samples. For the latter Gibbs sampler, we ran five chains in parallel; therefore alignment should be firstly carried out within each chain, then across chains.

4 Simulation

We simulated observed gene expression from the model we propose. Section 4.1 describes the data generation processes. We fitted the proposed model and a comparator model to the generated data. Section 4.2 introduces the model settings. We assessed the models’ performance in terms of estimating the correlation structure, predicting gene expressions, recovering factor trajectories and estimating factor loadings. Section 4.3 introduces the metrics we used for assessment and Section 4.4 discusses

models' performance using these metrics.

4.1 Simulation Setting

To mimic the real data (discussed in more detail in Section 5), we chose the sample size $n = 17$ and the true number of latent factors $k = 4$. The number of training and test time points was set to $u_1 = 8$ and $u_2 = 2$, respectively, for all individuals (i.e. we split the observed data into training and test datasets to assess models' performance in predicting gene expression). Since recovering latent factor trajectories is one of our major interests, we considered 4 different mechanisms for generating true latent factors according to a 2×2 factorial design: the first variable determined whether different factors were actually correlated ("C") or uncorrelated ("U"), and the second variable determined whether the variability of factors was small ("S") or large ("L"). The mean value for each factor score y_{ija} was fixed to be 0, and we generated the covariance matrix $\Sigma_{\mathbf{Y}}$ for different scenarios in the following way: (1) under scenario "C", we set the cross-correlation based on the estimated covariance matrix from real data under $k = 4$; otherwise under scenario "U" the true cross-correlation was set to be 0. (2) under scenario "S", we set the standard deviation for factors 1-4 to be 0.21, 0.23, 0.21, and 0.17, respectively, following the estimated results from real data under $k = 4$; while under scenario "L", the standard deviation for each y_{ija} was set to be 1. Below we use the factors' generation mechanism to name each scenario. For example, "scenario CS" refers to the case where true factors were correlated (C) and had small (S) variability.

Each factor was assumed to regulate 10% of all genes, and the total number of genes was $p = 100$. Note that we allow for the possibility that one gene may be regulated by more than one factor. If a gene was regulated by an underlying factor, then the corresponding factor loading was generated from a normal distribution $N(4, 1^2)$; otherwise the factor loading was set to 0. Each subject-gene mean μ_{ig} was generated from $N(\mu_g, \sigma_g^2)$, where μ_g ranged between 4 and 16 (to match the real data) and $\sigma_g = 0.5$. Finally, observed genes were generated according to Equation 1, $x_{ijg} \sim N(\mu_{ig} + \sum_{a=1}^k l_{ga} y_{ija}, \phi_g^2)$, where $\phi_g = 0.5$.

4.2 Analysis Methods

4.2.1 Setting of the Proposed Model

We fit the generated data using the proposed approach BSFA-DGP under different numbers of factors $k = 3, 4, 5$. The true number is usually unavailable in practice. Therefore, we investigate how the mis-specification of k impacts model performance. In our model, we specified $c_1 = d_1 = c_2 = d_2 = c_3 = d_3 = 10^{-2}$ for an uninformative Inverse-Gamma prior distribution for the variance terms. We

also set $c_0 = 10^{-1} \cdot p$ and $d_0 = (1 - 10^{-1}) \cdot p$ to obtain a sparsity-inducing prior on Z_{ga} , as the prior expectation of π_a under this specification is $\mathbb{E}[\pi_a] = \frac{c_0}{c_0 + d_0} = 10^{-1}$, implying that only 10% of genes are expected to be involved in each pathway. For the pre-specified values of m and W in the MCEM algorithm, we set the rate of sample size increase to $m = 2$ and the maximum number of attempts to increase the sample size to $W = 5$.

4.2.2 Comparator Model

To compare with traditional approaches modeling each latent factor independently, we also fit the data assuming an IGP prior for each factor trajectory \mathbf{y}_{ia} (other parts of the model remain unchanged); this model specification is referred to as BSFA-IGP.

4.2.3 Obtaining Good Initial Values

To provide good initial values for the MCEM algorithm, we implemented a two-step approach using available software. First, point estimates of latent factor scores y_{ija} were obtained via the BFRM software (described in Section 2.1). We centered the gene expression within each individual before inputting it into BFRM: the input data \mathbf{X}^c consisted of the centered x_{ijg}^c , $x_{ijg}^c = x_{ijg} - \frac{\sum_{j=1}^{q_i} x_{ijg}}{q_i}$. We did so because BFRM assumes independent data, therefore the intercept is specific to only a gene and not to a subject; in other words, it cannot estimate subject-gene mean μ_{ig} . Second, initial values of GP parameters were obtained by inputting \mathbf{Y} to GPFDA, with either a DGP or IGP specification.

4.3 Performance Metrics

4.3.1 Evaluation of MCEM Algorithm

We evaluated two aspects of the performance of MCEM. Firstly, we compared the final correlation estimate with the truth and secondly, we monitored the change in the correlation estimate throughout the whole iterative process, to assess the speed of convergence of the algorithm.

4.3.2 Assessment Of Convergence

Before summarising the posterior using Gibbs samples from five parallel chains, we assessed convergence of the continuous variables by Gelman-Rubin diagnostic (also known as Rhat) (Gelman and Rubin, 1992). Convergence of the latent factor scores y_{ija} and predictions of gene expression x_{ijg}^{new} were of particular interest. We used 1.2 as an empirical cutoff.

For factor loadings l_{ga} , which is the product of a binary variable Z_{ga} and a continuous variable A_{ga} , we first summarized the corresponding Z_{ga} : if the proportion of $Z_{ga} = 0$ exceeded 0.5 for all

chains, then l_{ga} was directly summarized as 0; otherwise $l_{ga} = A_{ga}$, and we assessed convergence for these factor loadings using Rhat.

Originally, for each chain, we set the total number of iterations to be 10,000, with 3000 burn-in iterations and retaining only every 10th iteration. However, we noticed that it was harder for factor scores y_{ija} and loadings l_{ga} to converge under certain cases: the “large variability” scenario for both DGP and IGP models, and the “small variability” scenario for only the IGP model. Therefore, for these cases we increased the number of iterations to 100,000, with 30,000 burn-in iterations and retaining only every 500th iteration. We list the largest Rhat for each variable type, x_{ijg}^{new} , y_{ija} , l_{ga} , in Supplementary Table 1. They reflect no apparent concerns over non-convergence.

4.3.3 Prediction of Gene Expression

We assessed the performance of predicting gene expressions using three metrics: mean absolute error ($\text{MAE}_{\mathbf{X}}$), mean width of the 95% predictive interval ($\text{MWI}_{\mathbf{X}}$), and proportion of genes within the 95% predictive interval ($\text{PWI}_{\mathbf{X}}$), which were calculated as:

$$\begin{aligned}\text{MAE}_{\mathbf{X}} &= \frac{\sum_{i=1}^n \sum_{j=u_1+1}^{u_1+u_2} \sum_{g=1}^p |x_{ijg}^{0.5} - x_{ijg}^{\text{true}}|}{nu_2p}, \\ \text{MWI}_{\mathbf{X}} &= \frac{\sum_{i=1}^n \sum_{j=u_1+1}^{u_1+u_2} \sum_{g=1}^p |x_{ijg}^{0.975} - x_{ijg}^{0.025}|}{nu_2p}, \\ \text{PWI}_{\mathbf{X}} &= \frac{\sum_{i=1}^n \sum_{j=u_1+1}^{u_1+u_2} \sum_{g=1}^p I(x_{ijg}^{0.025} < x_{ijg}^{\text{true}} < x_{ijg}^{0.975})}{nu_2p},\end{aligned}$$

where x_{ijg}^{true} denotes the true value of x_{ijg} , and $x_{ijg}^{0.025}, x_{ijg}^{0.5}, x_{ijg}^{0.975}$ denotes 2.5%, 50%, and 97.5% quantiles of the posterior samples, respectively; and $I(x_{ijg}^{0.025} < x_{ijg}^{\text{true}} < x_{ijg}^{0.975}) = 1$ if x_{ijg}^{true} is within the predictive interval, otherwise it is 0.

4.3.4 Recovery of Latent Factor Trajectories

To assess the performance in recovering factor trajectories underlying gene expression observed in the training data, we first present an overview of estimation results using the metric $\text{MAE}_{\mathbf{Y}}$:

$$\text{MAE}_{\mathbf{Y}} = \frac{\sum_{i=1}^n \sum_{j=1}^{u_1} \sum_{a=1}^k |y_{ija}^{0.5} - y_{ija}^{\text{true}}|}{nu_1k},$$

where y_{ija}^{true} is the true value of y_{ija} , and $y_{ija}^{0.5}$ is the 50% quantile of the posterior samples. In addition, we plot true and estimated factor trajectories for visual comparison. For the convenience of discussing results, we present trajectories for factor 1 of person 1 as an example. This chosen person-factor estimation result is representative of all factors of all people.

Note that in the scenarios CS and US, true $\text{vec}(\mathbf{Y}_i^T)$ was rescaled as $\mathbf{D}^{-1} \text{vec}(\mathbf{Y}_i^T)$ before the $\text{MAE}_{\mathbf{Y}}$ calculation, where \mathbf{D} is a diagonal matrix consisting of the square root of corresponding diagonal elements of the true covariance matrix $\Sigma_{\mathbf{Y}}$. This was to account for the difference in scale between the true and estimated factor trajectories caused by the unidentifiability of the factor covariance matrix, as discussed in Section 3.3. However, we did not apply such transformation when plotting the factor trajectories because the shape, in practice, can be estimated well, even though the true scale cannot be recovered.

4.3.5 Estimation of Factor Loadings

We evaluated the ability to estimate factor loadings from two perspectives. First, for a specific factor, could the model identify all genes that were truly affected by this factor? Second, for a specific gene, could the model identify all factors that regulate this gene? To answer these questions, we calculated 95% credible intervals for l_{gas} and presented those l_{gas} of which the interval did not contain 0 in the heatmap, using posterior median estimates. For the convenience of comparing estimates with the truth, true factor loadings under the scenarios CS and US were displayed after scaling by \mathbf{D} . Note that genes displayed in the heatmap are ordered following two rules: first, genes on factors with smaller indexes are ranked first; second, genes with larger absolute factor loadings are ranked first.

4.4 Results

4.4.1 Number of Factors Correctly Specified

When the number of latent factors k is correctly specified, the MCEM algorithm can recover the true auto-correlation and cross-correlation well. In terms of auto-correlation, DGP and IGP return similar results. The unique advantage of DGP over IGP is the ability to estimate cross-correlation. Under all data generation mechanisms considered, the algorithm returns satisfactory estimation of cross-correlation (Figure 2). We also present an example showing the evolution of cross-correlation estimates across iterations under the scenario CS in Supplementary Figure 2. The initial estimate (from the two-step approach) is poor, but MCEM is able to propose estimates that rapidly approximate the truth.

In terms of predicting gene expression, similar $\text{PWI}_{\mathbf{X}}$ is observed for both models. However, the DGP specification always leads to smaller $\text{MAE}_{\mathbf{X}}$ and narrower $\text{MWI}_{\mathbf{X}}$, even when the factors are uncorrelated in truth. This indicates more accuracy and less uncertainty in prediction (Table 1).

Summary results in Table 2 suggest that estimating factors is generally easier when the true variability of factors is larger. A closer inspection of factor trajectories delineated in Figure 3 further

confirms this: under scenarios CL and UL, both DGP and IGP models are able to recover the shape of factor trajectories very well. This could be explained by the relatively strong expression of latent factors. In contrast, in the case of CS and US, where expression is relatively weak, recovery of details of factor shapes is harder: if factors are not correlated at all (scenario US), both DGP and IGP fail to recover the details at the 2nd and 5th time point, though the overall shape is still close to the truth. However, if factors are truly correlated (scenario CS), DGP is able to recover trajectories very well, due to its ability to borrow information from other related factors.

With regard to factor loading estimation, Figure 4 shows results under the scenario CS, and Supplementary Figures 3-5 show results for the remaining scenarios. Both DGP and IGP perform well in the first task (identify the correct genes for a given factor) under all scenarios. However, for the second task (identify the correct factors for a given gene), although both models perform well under scenarios CL, UL and US, we observe that IGP performs less well under the scenario CS while DGP still performs well. As can be seen from Figure 4, IGP specification leads to the result that genes that are estimated to be significantly loaded on the first and second factor also significantly load on the fourth factor. One possible explanation for this is that, if in truth, factors have strong signals and/or are not correlated at all (corresponding to scenarios CL, UL and US), then it is relatively easy to distinguish contributions from different factors. In contrast, under the scenario CS where factors actually have weak signals and are highly-correlated (true correlation between factor 1 and 4 is -0.69 , and correlation between factor 2 and 4 is -0.71 , as can be found from Figure 2), it would be more difficult. DGP specification could greatly improve the estimation result as it explicitly takes the correlation among factors into consideration.

4.4.2 Number of Factors Misspecified

We also investigated the performance of our approach when the number of latent factors k is misspecified. The performance of BSFA-DGP in predicting gene expression is similar to when k is correctly specified (Supplementary Table 2). In addition, when k is misspecified to 5 (larger than the truth), the DGP model detected the redundant factor under all scenarios. Supplementary Figure 6 shows an example under scenario CL. In the estimated factor loading matrix, there is one factor with no genes significantly loaded on it, which indicates that a smaller k may suffice. In practice, we suggest users specify k as the upper limit of the expected number of latent factors initially, and decrease it accordingly if the result suggests redundancy.

5 Data Application

5.1 Data Description

The human challenge study described in Chen et al. (2011) is used as a real data example to illustrate the proposed approach. In this study, 17 healthy individuals were inoculated with the H3N2 influenza virus, and their blood samples were collected at regular time intervals until the individuals were discharged after a fixed period of 7 days. The blood samples were then assayed with DNA microarray technology, to produce gene expression values for 11,961 genes. Additionally, each participant was assigned a binary label based on a clinical assessment: symptomatic, or asymptomatic. This dataset will be called the “H3N2 data” below, and it is publicly available from this website.

5.2 Analysis Methods

To fit the BSFA-DGP model to the H3N2 data, we adopted the same constant parameters as that described in the simulation study. We ran 500,000 iterations for the final Gibbs sampler, with a 50% burn-in proportion and retained only every 100th iteration. We also compared our results with two alternative models, both of which assume independence between factors: the BSFA-IGP model, and a previous model in Chen et al. (2011), which adopted spline functions to model each factor trajectory independently.

5.3 Statistical Results

In terms of the prediction performance, similar $PWI_{\mathbf{X}}$ is observed under BSFA-DGP (0.951) and BSFA-IGP (0.956); whereas $MAE_{\mathbf{X}}$ and $MWI_{\mathbf{X}}$ are both smaller under BSFA-DGP ($MAE_{\mathbf{X}}$ 0.211; $MWI_{\mathbf{X}}$ 1.113) than BSFA-IGP ($MAE_{\mathbf{X}}$ 0.217; $MWI_{\mathbf{X}}$ 1.213). This again demonstrates the advantage of reducing prediction error and uncertainty if cross-correlations among factors are taken into consideration. With respect to the recovery of latent factors, both BSFA-DGP and BSFA-IGP have similar results, hence we will only discuss results under BSFA-DGP below and compare them with those in Chen et al. (2011).

Estimated factor trajectories are displayed in Figure 5. Among all, factor 1 is able to distinguish symptomatic people from asymptomatic people most clearly, therefore we investigate this factor further. We find that its shape is largely similar to the “principal factor” identified in Chen et al. (2011). To facilitate comparison, Figure 6 displays the factor trajectory for all people in the same format as Figure 4 in Chen et al. (2011). For symptomatic people, both factors display an increase after the inoculation (time 0), then decrease to a level that is higher than before-inoculation; but for asymptomatic people, both factor shapes have little change.

In addition to the shape similarity, genes significantly loaded on factor 1 are also largely similar to those loaded on Chen et al. (2011)’s principal factor. Chen et al. (2011) list the top 50 genes sorted according to the absolute loading values (from most important to least important); we present this alongside the full list of our top 50 genes in Supplementary Table 3 for comparison. 33 out of the 50 genes are the same.

Despite the similarity between factor 1 estimated by our BSFA-DGP and the principal factor estimated by Chen et al. (2011), as discussed above, it is noteworthy that the trajectory of factor 1 is actually more individualized and informative than the principal factor. This can be seen by observing that, for symptomatic people, the shapes of the principal factor are exactly the same after the factor starts changing (Figure 4 in Chen et al. (2011)) whereas the shapes of factor 1 still vary locally for different subjects, as can be seen from Figure 6. This difference is caused by the different assumptions underlying the two models. Chen et al. (2011) assume that the dynamic trajectory of any factor is common to all individuals. Different factor values are observed at the same time point for different people only due to individual-dependent biological time shifts and random noise. Therefore, symptomatic and asymptomatic individuals are distinguished based on the time shift (Figure 4 in Chen et al. (2011)). In contrast, we assume that the trajectory of each factor comes from a distribution (i.e., there is no common curve for every individual), therefore allowing for different curve shapes for different people. We make direct use of the diversity of curve shapes to distinguish patients without introducing the “time shift” quantity.

5.4 Biological Interpretation

To identify the biological counterpart (i.e., pathway) of the statistical factor, we used the KEGG Pathway analysis of the online bioinformatics platform DAVID. We uploaded the total 11,961 genes as the “Background” and the top 50 genes loaded on factor 1 as the “Gene List”.

Results show that these selected genes are significantly enriched on several pathways, including the pathways associated with Influenza A and Covid-19 (see Supplementary Figure 7 for a full list of pathway results returned by DAVID). What these pathways have in common is that they are all related to human innate immune and inflammatory response. This suggests that the genes selected by our model play important roles during the biological processes of detecting viral RNA and initiating an immune and inflammatory response, which is as expected because the data we analyze comes from a viral infection study.

6 Discussion

In this paper we propose a BSFA-DGP model, which relaxes the classical assumption of independent factors when mapping the high-dimensional gene expressions to low-dimensional latent factor representations. By borrowing information from correlated factor trajectories, this model has demonstrated advantages in both gene expression prediction and latent factor recovery compared to other models.

It is worth mentioning that, although the proposed model was motivated by the specific context of gene-pathway relationship, it can be applied to other fields where such latent factor structure exists. For example, in Alzheimer’s disease, three latent dimensions (cerebral anatomy, cognitive ability and functional autonomy) have been defined underlying six measured markers based on previous knowledge (see Figure 1 in Taddé et al. (2020) for more details). Understanding how these dimensions change over time according to the clinical stage is of interest in Alzheimer’s research. Our model can be applied in this case to infer both the trajectories of the latent dimensions and the factor loading structure directly from data, which may discover factors that were not identified previously.

We also develop an MCEM algorithm for the inference of the model; the main motivation for adopting this algorithm is that it can make full use of the existing package to estimate DGP parameters. In the M-step of MCEM, GPFDA can be directly implemented to find the maximizer of the Q-function; thus we can exploit the existing optimization algorithm. In addition to its implementation convenience, the modular structure of the MCEM framework makes it generalizable to other complex models involving the DGP model component. MCEM comprises two relatively simple parts: one is to obtain empirical estimates of DGP parameters Θ given Monte Carlo samples of \mathbf{Y} (M-step), using the GPFDA package; the other is to generate samples \mathbf{Y} under a fixed estimate of Θ (E-step), using a standard MCMC sampler. For example, when using a DGP model for the latent continuous variable introduced to model multivariate dependent, non-continuous data (such as binary or count data), Shi et al. (2017) used Laplace Approximation; the MCEM framework we develop would be an alternative inference approach in this case.

Computation time of our approach is largely dependent on GPFDA, which returns hyperparameter estimates for the DGP to maximize the exact likelihood of observing the inputs \mathbf{Y} . GPFDA does not scale well with n , and this means our approach does not scale well with sample size. Simulation results showed that the algorithm could not end within 36 hours once n was larger than 500. Potential solutions to this scalability issue include the model approximation methods proposed in Alvarez and Lawrence (2011), or variational inference discussed in Titsias (2009); Álvarez et al. (2010); Hensman et al. (2013). However, our approach does scale well with p : our MCEM algorithm took around 1.5 hours for the real data in Section 5 and 4 minutes for the simulated data in Section 4 on a standard

laptop (Quad-Core Intel Core i5). The good scaling in p is because the number of latent factors k input to GPFDA is always small regardless of the number of the biomarkers.

Throughout this paper, several assumptions were made in the model, and below we will discuss how they could be relaxed in future work. First, when using GPs to model latent factor trajectories, we assume the mean function to be 0. In practice, if prior knowledge suggests that there are covariates that may affect the pathway-level expression, we could easily incorporate these covariates to model the mean function of GP (Shi and Choi, 2011). This extension will not change the original covariance structure imposed on the latent trajectories, therefore the MCEM framework will still work for this modified model. In addition, if there is prior knowledge that one or more of the latent factors have a particular shape, then this shape can be described by the mean functions of the relevant GPs. For example, if it is a priori known that the cell cycle pathway is involved, then the mean function can be chosen to have a sinusoidal shape to capture this information.

Another assumption is that the impact of latent factors on genes is time-invariant (i.e., factor loading \mathbf{L} is constant across all time points). This assumption may not be satisfied in practice; a potential solution would be to use Hidden Markov Models (Song et al., 2017) to introduce a hidden, discrete variable that varies with time, of which different states correspond to different factor loading matrices.

In addition, the number of latent factors k was fixed and needed to be pre-specified. Though results of our model was able to infer redundant factors (as demonstrated in the simulation study), an automatic approach to infer this number from the data may be preferable in some contexts. A potential solution would be to introduce the Indian Buffet Process as a prior distribution over equivalence classes of infinite-dimensional binary matrices (Ghahramani and Griffiths, 2005; Knowles and Ghahramani, 2011).

7 Software

The R code used for implementing the proposed BSFA-DGP model is available as an R package, DGP4LCF, on Github: <https://github.com/jcai-1122/DGP4LCF>. The package contains vignettes, which illustrate the usage of the functions within the package by applying them to analyze simulated dataset. The release used in this paper is available at <https://doi.org/10.5281/zenodo.8108150>.

Acknowledgments

This work is supported through the United Kingdom Medical Research Council programme grants MC_UU_00002/2 and MC_UU_00002/20. The authors are grateful to Oscar Rueda for the helpful discus-

sion on the bioinformatics side of the project.

Conflict of Interest: None declared.

References

- Álvarez, M., Luengo, D., Titsias, M., and Lawrence, N. D. (2010). Efficient multioutput gaussian processes through variational inducing kernels. In *Proceedings of the Thirteenth International Conference on Artificial Intelligence and Statistics*, pages 25–32. JMLR Workshop and Conference Proceedings.
- Alvarez, M. A. and Lawrence, N. D. (2011). Computationally efficient convolved multiple output Gaussian processes. *The Journal of Machine Learning Research*, 12:1459–1500.
- Bekker, P. A. and ten Berge, J. M. (1997). Generic global indentation in factor analysis. *Linear Algebra and its Applications*, 264:255–263.
- Bernardo, J., Bayarri, M., Berger, J., Dawid, A., Heckerman, D., Smith, A., and West, M. (2003). Bayesian factor regression models in the “large p, small n” paradigm. *Bayesian Statistics*, 7:733–742.
- Bhattacharya, A. and Dunson, D. B. (2011). Sparse Bayesian infinite factor models. *Biometrika*, 98(2):291–306.
- Bonilla, E. V., Chai, K., and Williams, C. (2007). Multi-task Gaussian process prediction. *Advances in Neural Information Processing Systems*, 20.
- Booth, J. G. and Hobert, J. P. (1999). Maximizing generalized linear mixed model likelihoods with an automated Monte Carlo EM algorithm. *Journal of the Royal Statistical Society: Series B (Statistical Methodology)*, 61(1):265–285.
- Boyle, P. and Frean, M. (2005a). Dependent Gaussian processes. *Advances in Neural Information Processing Systems*, 17:217–224.
- Boyle, P. and Frean, M. (2005b). Multiple output Gaussian process regression.
- Caffo, B. S., Jank, W., and Jones, G. L. (2005). Ascent-based Monte Carlo expectation–maximization. *Journal of the Royal Statistical Society: Series B (Statistical Methodology)*, 67(2):235–251.
- Caruana, R. (1997). Multitask learning. *Machine learning*, 28(1):41–75.
- Carvalho, C. M., Chang, J., Lucas, J. E., Nevins, J. R., Wang, Q., and West, M. (2008). High-dimensional sparse factor modeling: applications in gene expression genomics. *Journal of the American Statistical Association*, 103(484):1438–1456.

- Casella, G. (2001). Empirical Bayes Gibbs sampling. *Biostatistics*, 2(4):485–500.
- Chen, M., Zaas, A., Woods, C., Ginsburg, G. S., Lucas, J., Dunson, D., and Carin, L. (2011). Predicting viral infection from high-dimensional biomarker trajectories. *Journal of the American Statistical Association*, 106(496):1259–1279.
- Conti, G., Frühwirth-Schnatter, S., Heckman, J. J., and Piatek, R. (2014). Bayesian exploratory factor analysis. *Journal of econometrics*, 183(1):31–57.
- Dempster, A. P., Laird, N. M., and Rubin, D. B. (1977). Maximum likelihood from incomplete data via the EM algorithm. *Journal of the Royal Statistical Society: Series B (Methodological)*, 39(1):1–22.
- Dey, D., Datta, A., and Banerjee, S. (2020). Graphical Gaussian process models for highly multivariate spatial data. *arXiv preprint arXiv:2009.04837*.
- Gelman, A. and Rubin, D. B. (1992). Inference from iterative simulation using multiple sequences. *Statistical Science*, pages 457–472.
- Genton, M. G. and Kleiber, W. (2015). Cross-covariance functions for multivariate geostatistics. *Statistical Science*, 30(2):147–163.
- Ghahramani, Z. and Griffiths, T. (2005). Infinite latent feature models and the Indian buffet process. *Advances in Neural Information Processing Systems*, 18.
- Guan, Y. and Haran, M. (2019). Fast expectation-maximization algorithms for spatial generalized linear mixed models. *arXiv preprint arXiv:1909.05440*.
- Havasi, M., Hernández-Lobato, J. M., and Murillo-Fuentes, J. J. (2018). Inference in deep Gaussian processes using stochastic gradient Hamiltonian Monte Carlo. *Advances in Neural Information Processing Systems*, 31.
- Hensman, J., Fusi, N., and Lawrence, N. D. (2013). Gaussian processes for big data. *arXiv preprint arXiv:1309.6835*.
- Hsu, C.-L. and Yang, U.-C. (2012). Discovering pathway cross-talks based on functional relations between pathways. *BMC Genomics*, 13(7):1–15.
- Jones, G. L. (2004). On the Markov chain central limit theorem. *Probability Surveys*, 1:299–320.
- Kim, S. Y., Choe, E. K., Shivakumar, M., Kim, D., and Sohn, K.-A. (2021). Multi-layered network-based pathway activity inference using directed random walks: application to predicting clinical outcomes in urologic cancer. *Bioinformatics*, 37(16):2405–2413.

- Knowles, D. and Ghahramani, Z. (2011). Nonparametric bayesian sparse factor models with application to gene expression modeling.
- Konzen, E., Cheng, Y., and Shi, J. Q. (2021). Gaussian process for functional data analysis: The GPFDA package for R. *arXiv preprint arXiv:2102.00249*.
- Ledermann, W. (1937). On the rank of the reduced correlational matrix in multiple-factor analysis. *Psychometrika*, 2(2):85–93.
- Levine, R. A. and Casella, G. (2001). Implementations of the Monte Carlo EM algorithm. *Journal of Computational and Graphical Statistics*, 10(3):422–439.
- Levine, R. A. and Fan, J. (2004). An automated (Markov chain) Monte Carlo EM algorithm. *Journal of Statistical Computation and Simulation*, 74(5):349–360.
- Liu, H., Cai, J., and Ong, Y.-S. (2018). Remarks on multi-output Gaussian process regression. *Knowledge-Based Systems*, 144:102–121.
- Lunn, D., Jackson, C., Best, N., Thomas, A., and Spiegelhalter, D. (2013). The BUGS book. *A Practical Introduction to Bayesian Analysis*, Chapman Hall, London.
- Molstad, A. J., Hsu, L., and Sun, W. (2021). Gaussian process regression for survival time prediction with genome-wide gene expression. *Biostatistics*, 22(1):164–180.
- Neath, R. C. (2013). On convergence properties of the Monte Carlo EM algorithm. In *Advances in modern statistical theory and applications: a Festschrift in Honor of Morris L. Eaton*, pages 43–62. Institute of Mathematical Statistics.
- Newton, M. A. and Raftery, A. E. (1994). Approximate Bayesian inference with the weighted likelihood bootstrap. *Journal of the Royal Statistical Society: Series B (Methodological)*, 56(1):3–26.
- Papastamoulis, P. and Ntzoufras, I. (2022). On the identifiability of Bayesian factor analytic models. *Statistics and Computing*, 32(2):1–29.
- Penny, W. and Roberts, S. (2002). Bayesian multivariate autoregressive models with structured priors. *IEE Proceedings-Vision, Image and Signal Processing*, 149(1):33–41.
- Ramsay, J. and Hooker, G. (2019). *Dynamic data analysis: modeling data with differential equations*. Springer.
- Ramsay, J., Hooker, G., and Graves, S. (2009). Introduction to functional data analysis. In *Functional data analysis with R and MATLAB*, pages 1–19. Springer.

- Richardson, S., Tseng, G. C., and Sun, W. (2016). Statistical methods in integrative genomics. *Annual review of statistics and its application*, 3:181.
- Shi, J. Q., Cao, C., et al. (2017). Regression analysis for multivariate dependent count data using convolved Gaussian processes. *arXiv preprint arXiv:1710.01523*.
- Shi, J. Q. and Choi, T. (2011). *Gaussian process regression analysis for functional data*. CRC Press.
- Song, X., Xia, Y., and Zhu, H. (2017). Hidden Markov latent variable models with multivariate longitudinal data. *Biometrics*, 73(1):313–323.
- Taddé, B. O., Jacqmin-Gadda, H., Dartigues, J.-F., Commenges, D., and Proust-Lima, C. (2020). Dynamic modeling of multivariate dimensions and their temporal relationships using latent processes: Application to Alzheimer’s disease. *Biometrics*, 76(3):886–899.
- Temate-Tiagueu, Y., Seesi, S. A., Mathew, M., Mandric, I., Rodriguez, A., Bean, K., Cheng, Q., Glebova, O., Măndoiu, I., Lopanik, N. B., et al. (2016). Inferring metabolic pathway activity levels from RNA-Seq data. *BMC Genomics*, 17(5):493–503.
- Titsias, M. (2009). Variational learning of inducing variables in sparse gaussian processes. In *Artificial intelligence and statistics*, pages 567–574. PMLR.
- Vaske, C. J., Benz, S. C., Sanborn, J. Z., Earl, D., Szeto, C., Zhu, J., Haussler, D., and Stuart, J. M. (2010). Inference of patient-specific pathway activities from multi-dimensional cancer genomics data using paradigm. *Bioinformatics*, 26(12):i237–i245.
- Wang, X., Sun, Z., Zimmermann, M. T., Bugrim, A., and Kocher, J.-P. (2019). Predict drug sensitivity of cancer cells with pathway activity inference. *BMC Medical Genomics*, 12(1):5–13.
- Wei, G. C. and Tanner, M. A. (1990). A Monte Carlo implementation of the EM algorithm and the poor man’s data augmentation algorithms. *Journal of the American Statistical Association*, 85(411):699–704.
- Wu, C. J. (1983). On the convergence properties of the EM algorithm. *The Annals of Statistics*, pages 95–103.

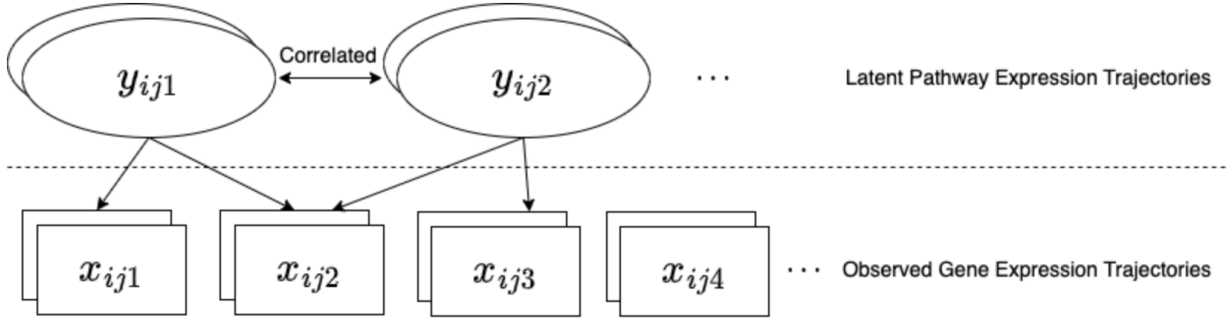


Figure 1: Illustration of the motivating data structure. The “Observed Gene Expression Trajectories” consists of longitudinal gene expression x_{ijg} , where i, j, g is the index for person, time, and gene, respectively; the rectangles behind the text box indicate that measurements are taken longitudinally (more than one time point). The “Latent Pathway Expression Trajectories” comprise time-evolving pathway expression y_{ija} , where i, j, a is the index for person, time, and pathway, respectively; the ovals behind the text box suggest that pathway expression is also time-evolving. The ellipses “...” represent additional genes and pathways that are omitted here. The dashed line is used to separate the “Observed Gene Expression Trajectories” and the “Latent Pathway Expression Trajectories”.

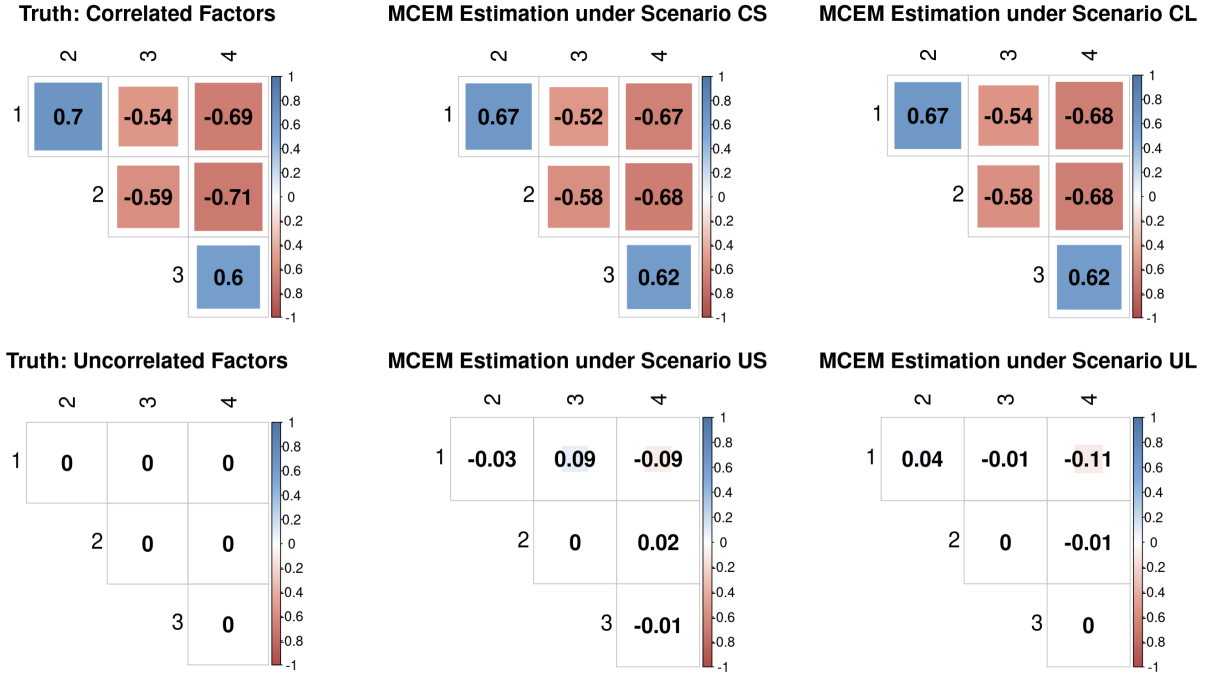


Figure 2: Comparison between true and estimated cross-correlation matrices using the DGP model: all scenarios, number of latent factors k correctly specified as 4. The first column displays true correlation, while the second and third columns display estimates. The first and second row show values under correlated and uncorrelated factors, respectively.

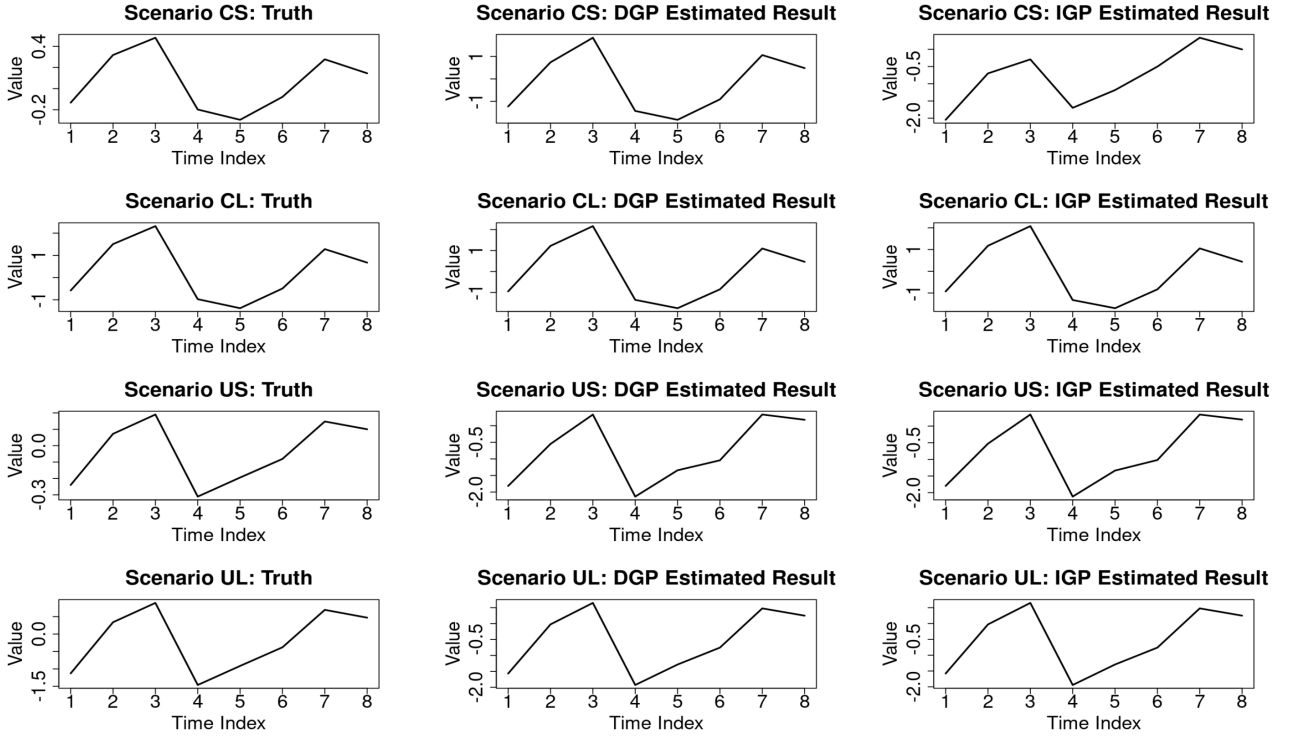


Figure 3: Comparison between true and estimated latent factor trajectory for factor 1 of person 1: all scenarios, number of latent factors k correctly specified as 4. Each row corresponds to a data generation mechanism, with the first column displaying truth, the second column displaying DGP estimated result and the third column displaying IGP estimated result.

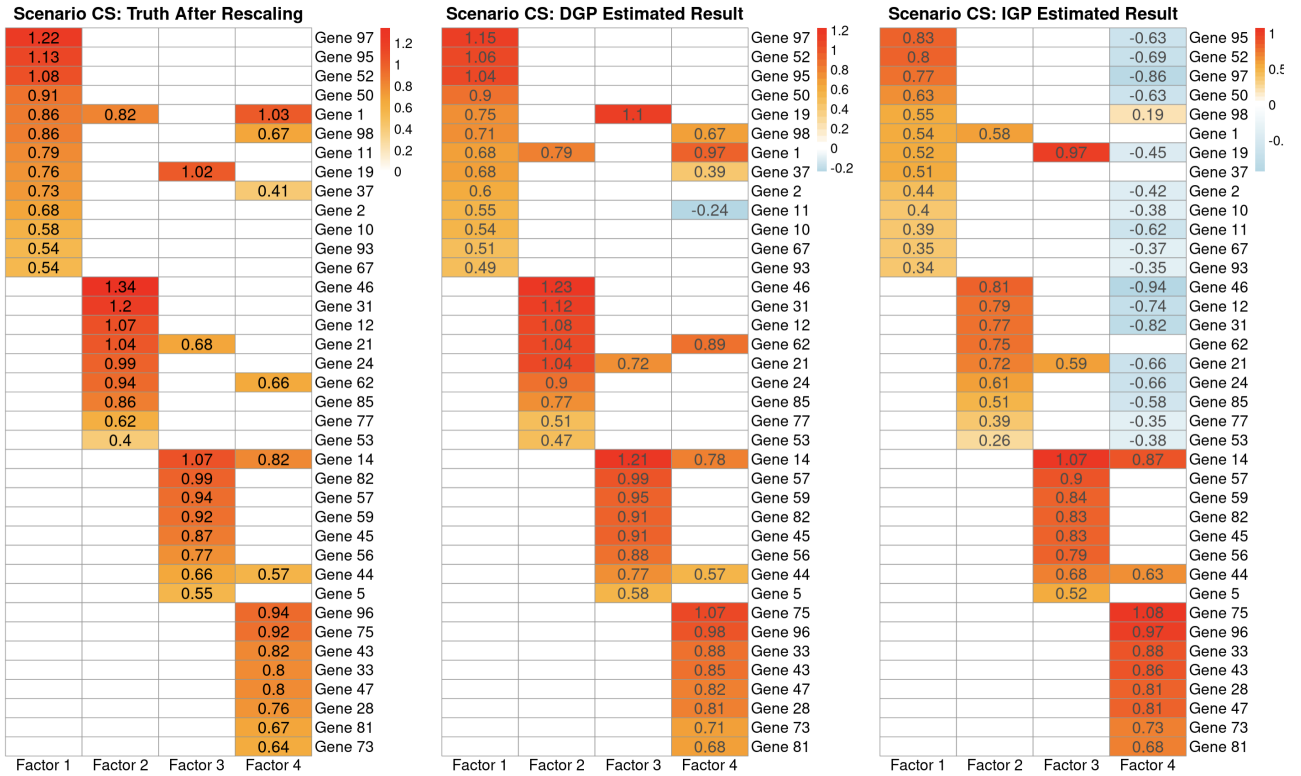


Figure 4: Comparison between true and estimated factor loadings: scenario CS, with the number of latent factors k correctly specified as 4. Genes displayed in each heatmap are ordered following the same two rules: first, genes on factors with smaller indexes are ranked first; second, genes with larger absolute factor loadings are ranked first.

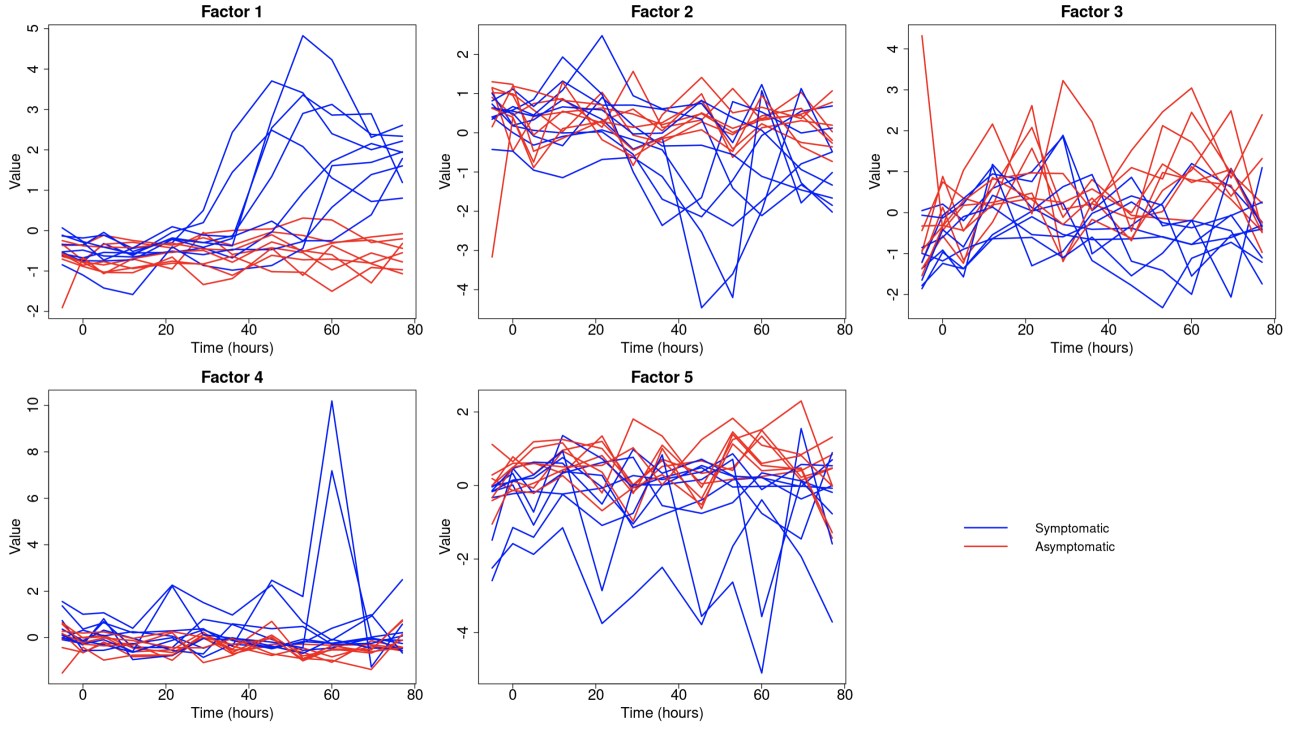


Figure 5: Estimated trajectories for all factors in the H3N2 data. Each panel displays all subjects' trajectories for a single factor.

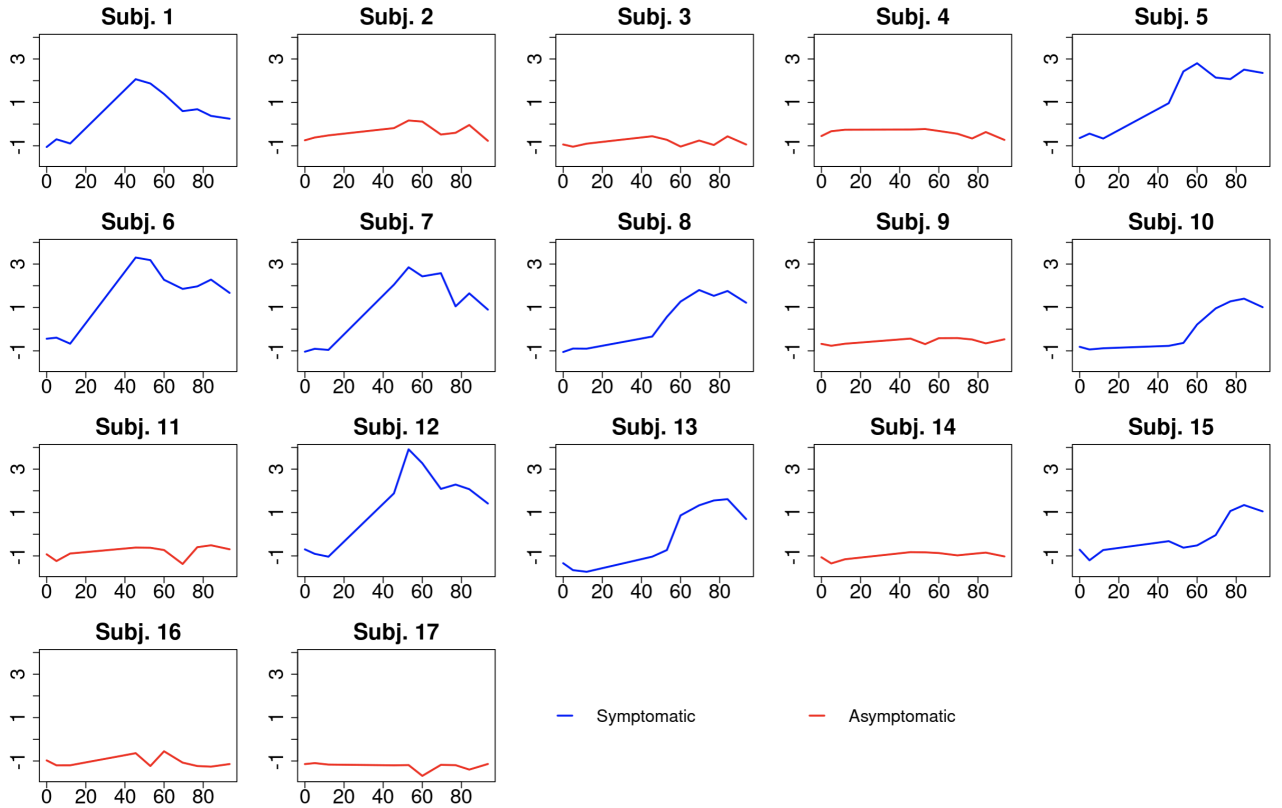


Figure 6: Estimated trajectories for factor 1 in the H3N2 data. Each panel displays a single subject's trajectory, following the same format as Figure 4 in Chen et al. (2011). The horizontal axes correspond to time in hours.

Algorithm 1: MCEM Algorithm for the MLE of DGP Parameters.

Input : Observed gene expression \mathbf{X}_i and time points \mathbf{t}_i , $i = 1, \dots, n$ for n people.

Output: The MLE of DGP parameters $\hat{\Theta}^{\text{MLE}}$.

1 Step 1: Initialization Step

- Center \mathbf{X}_i to obtain \mathbf{X}_i^c (as defined in Section 4.2.3), which is input to BFRM for \mathbf{Y}^0 .
- Input \mathbf{Y}^0 to GPFDA for $\hat{\Theta}^{(0)}$, and construct $\hat{\Sigma}_{\mathbf{Y}}^{(0)}$ using $\hat{\Theta}^{(0)}$ and $\mathbf{t} = \bigcup_{i=1}^n \mathbf{t}_i$.
- Initialize the starting sample size $R^{(0)}$; the counter $w = 0$, which counts the total number of sample size increase, and specify its upper limit as W as described in Section 3.1.4.

Step 2: Iteration Step, Starting from $l = 1$

do

- 2.1 Draw $R^{(l-1)}$ samples of Ω from the Gibbs sampler $f(\Omega|\mathbf{X}, \hat{\Sigma}_{\mathbf{Y}}^{(l-1)})$ in Section 3.2, where $\hat{\Sigma}_{\mathbf{Y}}^{(l-1)}$ is constructed by $\hat{\Theta}^{(l-1)}$ and \mathbf{t} .
- 2.2 Retain $R_{\text{remain}}^{(l-1)}$ samples by discarding burn-in and thinning.
- 2.3 Align post-processed samples $\{\mathbf{L}^r, \mathbf{Y}_i^r\}_{r=1, \dots, R_{\text{remain}}^{(l-1)}}$ using R package “factor.switch”.
- 2.4 Input aligned samples $\{\mathbf{Y}_i^r\}_{r=1, \dots, R_{\text{remain}}^{(l-1)}}$ to GPFDA to obtain $\hat{\Sigma}_{\mathbf{Y}}^{(l)}$.
- 2.5 Calculate the lower bound proposed by Caffo et al. (2005) using $\hat{\Sigma}_{\mathbf{Y}}^{(l-1)}$, $\hat{\Sigma}_{\mathbf{Y}}^{(l)}$ and $\{\mathbf{Y}_i^r\}_{r=1, \dots, R_{\text{remain}}^{(l-1)}}$ (see Section A.3.2. of the supplementary materials for details).

if $LB > 0$ then

$R^{(l)} \leftarrow R^{(l-1)}$;
 $l \leftarrow l + 1$;

else

$R^{(l-1)} \leftarrow R^{(l-1)} + \frac{R^{(l-1)}}{m}$;
 $w \leftarrow w + 1$;

while $w \leq W$;

Table 1: Prediction results for all scenarios: number of latent factors k correctly specified as 4 for both DGP and IGP models. $\text{MAE}_{\mathbf{X}}$, $\text{MWI}_{\mathbf{X}}$ and $\text{PWI}_{\mathbf{X}}$ are short for mean absolute error, mean width of the 95% predictive intervals, and the proportion of genes within 95% the predictive intervals, respectively.

Factor Generation Mechanism		DGP, $k = 4$			IGP, $k = 4$		
Correlation	Variability	$\text{MAE}_{\mathbf{X}}$	$\text{MWI}_{\mathbf{X}}$	$\text{PWI}_{\mathbf{X}}$	$\text{MAE}_{\mathbf{X}}$	$\text{MWI}_{\mathbf{X}}$	$\text{PWI}_{\mathbf{X}}$
Correlated	Large	1.29	6.52	0.95	1.42	7.85	0.95
	Small	0.53	2.66	0.95	0.55	2.76	0.95
Uncorrelated	Large	1.44	7.28	0.95	1.53	7.70	0.95
	Small	0.55	2.78	0.95	0.56	2.79	0.95

Table 2: Estimation results for all scenarios: number of latent factors k correctly specified as 4 for both DGP and IGP model. $\text{MAE}_{\mathbf{Y}}$ is short for mean absolute error of estimating latent factors \mathbf{Y} .

Factor Generation Mechanism		$\text{MAE}_{\mathbf{Y}}$	
Correlation	Variability	DGP	IGP
Correlated	Large	0.15	0.16
	Small	0.23	0.41
Uncorrelated	Large	0.16	0.17
	Small	0.23	0.23

Supplementary Materials

A. Mathematical Derivations

A.1. Full Conditionals of the Gibbs Sampler for the Proposed Model

Throughout the following derivation, “o” denotes element-wise multiplication, “−” denotes observed data and all parameters in the model other than the parameter under derivation, “ $\|\mathbf{z}\|^2$ ” denotes the sum of squares of each element of the vector \mathbf{z} , “ $\text{diag}(\mathbf{z})$ ” denotes a diagonal matrix with the vector \mathbf{z} as its main diagonal elements, “ $\text{MVN}(\mathbf{z}; \boldsymbol{\mu}_{\mathbf{z}}, \Sigma_{\mathbf{z}})$ ” denotes that \mathbf{z} follows a multivariate normal distribution with mean $\boldsymbol{\mu}_{\mathbf{z}}$, and variance $\Sigma_{\mathbf{z}}$, and similar interpretations apply to other distributions. “ \mathbf{z}^T ” denotes the transpose of the vector or matrix \mathbf{z} , and “pos” is short for ‘posterior probability’.

- Full conditional for the latent factors $\text{vec}(\mathbf{Y}_i^T), i = 1, \dots, n$

$$f(\text{vec}(\mathbf{Y}_i^T)|-) = f(\text{vec}(\mathbf{Y}_{i,\text{obs}}^T)|-) \cdot f(\text{vec}(\mathbf{Y}_{i,\text{miss}}^T)|\text{vec}(\mathbf{Y}_{i,\text{obs}}^T), \Sigma_{\mathbf{Y}})$$

We first sample for $\text{vec}(\mathbf{Y}_{i,\text{obs}}^T)$:

$$\begin{aligned} f(\text{vec}(\mathbf{Y}_{i,\text{obs}}^T)|-) &\propto \text{MVN}(\text{vec}(\mathbf{X}_i^T); \text{vec}(\mathbf{M}_i^T) + \mathbf{L}_i^* \text{vec}(\mathbf{Y}_{i,\text{obs}}^T), \Sigma_{\mathbf{X}_i}) \cdot \text{MVN}(\text{vec}(\mathbf{Y}_{i,\text{obs}}^T); \mathbf{0}, \Sigma_{\mathbf{Y}_{i,\text{obs}}}) \\ &= \text{MVN}(\mu_{\mathbf{Y}_{i,\text{obs}}}^{\text{pos}}, \Sigma_{\mathbf{Y}_{i,\text{obs}}}^{\text{pos}}), \end{aligned}$$

with

$$\begin{aligned} \Sigma_{\mathbf{Y}_{i,\text{obs}}}^{\text{pos}} &= [\mathbf{L}_i^{*T} \Sigma_{\mathbf{X}_i}^{-1} \mathbf{L}_i^* + \Sigma_{\mathbf{Y}_{i,\text{obs}}}^{-1}]^{-1} \\ \mu_{\mathbf{Y}_{i,\text{obs}}}^{\text{pos}} &= \Sigma_{\mathbf{Y}_{i,\text{obs}}}^{\text{pos}} (\mathbf{L}_i^{*T} \Sigma_{\mathbf{X}_i}^{-1} (\text{vec}(\mathbf{X}_i^T) - \text{vec}(\mathbf{M}_i^T))). \end{aligned}$$

Then we sample for $\text{vec}(\mathbf{Y}_{i,\text{miss}}^T)$ from $f(\text{vec}(\mathbf{Y}_{i,\text{miss}}^T)|\text{vec}(\mathbf{Y}_{i,\text{obs}}^T), \Sigma_{\mathbf{Y}})$, a MVN distribution due to the property of the DGP model.

In the above equations:

- $\Sigma_{\mathbf{Y}}$ is the covariance matrix of factor scores at full time \mathbf{t} , and $\Sigma_{\mathbf{Y}_{i,\text{obs}}}$ is a sub-matrix of it (at subject-specific time points);
- \mathbf{L}_i^* is constructed using components of the factor loading matrix \mathbf{L} : $\mathbf{L}_i^* = (\mathbf{L}_1^*, \dots, \mathbf{L}_p^*)^T \in \mathbb{R}^{pq_i \times kq_i}$, where $(\mathbf{L}_g^*)^T = (\text{diag}(l_{g1})_{q_i \times q_i}, \dots, \text{diag}(l_{gp})_{q_i \times q_i}) \in \mathbb{R}^{q_i \times kq_i}$;

- $\Sigma_{\mathbf{X}_i} = \text{diag}((\phi_1^2)_{\times q_i}, \dots, (\phi_p^2)_{\times q_i}) \in \mathbb{R}^{pq_i \times pq_i}$, where $(\phi_a^2)_{\times q_i}$ represents a q_i -dimensional row vector consisting of the scalar ϕ_a^2 .

Note that when coding the algorithm, there is no need to really create the $pq_i \times pq_i$ diagonal matrix $\Sigma_{\mathbf{X}_i}^{-1}$ as the memory will be exhausted. To calculate the term $\mathbf{L}_i^{*T} \Sigma_{\mathbf{X}_i}^{-1}$, we can use the property of multiplication of a diagonal matrix: post-multiplying a diagonal matrix is equivalent to multiplying each column of the first matrix by corresponding elements in the diagonal matrix.

- Full conditional for the binary matrix \mathbf{Z}

Let $\mathbf{Z}_{g\cdot} = (Z_{g1}, \dots, Z_{gk})$ denote the g th row of the matrix \mathbf{Z} , $g = 1, \dots, p$; then,

$$f(\mathbf{Z}_{g\cdot} | -) \propto \prod_{i=1}^n \text{MVN}(\mathbf{x}_{ig}; \boldsymbol{\mu}_{ig} + (\mathbf{A}_{g\cdot} \circ \mathbf{Z}_{g\cdot}) \mathbf{Y}_i, \text{diag}(\phi_g^2, q_i)) \cdot \prod_{a=1}^k \text{Bernoulli}(Z_{ga}; \pi_a),$$

We calculate the posterior probability under 2^k possible values of $\mathbf{Z}_{g\cdot}$ based on the above formula, then sample with corresponding probability.

- Full conditional for the regression coefficient matrix \mathbf{A}

Let $\mathbf{A}_{g\cdot} = (A_{g1}, \dots, A_{gk})$ denote the g th row of the matrix \mathbf{A} , $g = 1, \dots, p$; then,

$$\begin{aligned} f(\mathbf{A}_{g\cdot} | -) &\propto \prod_{i=1}^n \text{MVN}(\mathbf{x}_{ig}; \boldsymbol{\mu}_{ig} + (\mathbf{A}_{g\cdot} \circ \mathbf{Z}_{g\cdot}) \mathbf{Y}_i, \text{diag}(\phi_g^2, q_i)) \cdot \text{MVN}(\mathbf{A}_{g\cdot}; \mathbf{0}, \text{diag}(\boldsymbol{\rho}^2)) \\ &= \text{MVN}(\mathbf{A}_{g\cdot}; \boldsymbol{\mu}_{\mathbf{A}_{g\cdot}}^{\text{pos}}, \Sigma_{\mathbf{A}_{g\cdot}}^{\text{pos}}), \end{aligned}$$

where

$$\begin{aligned} \Sigma_{\mathbf{A}_{g\cdot}}^{\text{pos}} &= \left(\frac{\text{diag}(\mathbf{Z}_{g\cdot}) (\sum_{i=1}^n \mathbf{Y}_i^T \mathbf{Y}_i) \text{diag}(\mathbf{Z}_{g\cdot})}{\phi_g^2} + \text{diag}\left(\frac{1}{\boldsymbol{\rho}^2}\right) \right)^{-1} \\ \boldsymbol{\mu}_{\mathbf{A}_{g\cdot}}^{\text{pos}} &= \frac{\Sigma_{\mathbf{A}_{g\cdot}} (\text{diag}(\mathbf{Z}_{g\cdot}) \sum_{i=1}^n \mathbf{Y}_i (\mathbf{x}_{ig} - \boldsymbol{\mu}_{ig}))}{\phi_g^2}. \end{aligned}$$

and $\boldsymbol{\rho}^2 = (\rho_1^2, \dots, \rho_a^2)$.

- Full conditional for the intercept $\mu_{ig}, i = 1, \dots, n; g = 1, \dots, p$

$$\begin{aligned} f(\mu_{ig} | -) &\propto \prod_{j=1}^{q_i} \text{N}(x_{ijg}; \mu_{ig} + \sum_{a=1}^k l_{ga} y_{ija}, \phi_g^2) \cdot \text{N}(\mu_{ig}; \mu_g, \sigma_g^2) \\ &= \text{N}(\mu_{ig}; \mu_{ig}^{\text{pos}}, \sigma_{ig}^{2, \text{pos}}), \end{aligned}$$

where

$$\sigma_{ig}^{2,\text{pos}} = \left(\frac{1}{\sigma_g^2} + \frac{q_i}{\phi_g^2} \right)^{-1}$$

$$\mu_{ig}^{\text{pos}} = \left(\frac{\mu_g}{\sigma_g^2} + \frac{\sum_{j=1}^{q_i} (x_{ijg} - \sum_{a=1}^k l_{ga} y_{ija})}{\phi_g^2} \right) \cdot \sigma_{ig}^{2,\text{pos}}$$

- Full conditional for π_a , $a = 1, \dots, k$

$$f(\pi_a | -) \propto \prod_{a=1}^k \text{Bernoulli}(Z_{ga}; \pi_a) \cdot \text{Beta}(\pi_a; c_0, d_0)$$

$$= \text{Beta}(c_0 + \sum_{g=1}^p Z_{ga}, d_0 + \sum_{g=1}^p (1 - Z_{ga}))$$

- Full conditional for ρ_a^2 , $a = 1, \dots, k$

$$f(\rho_a^2 | -) \propto \prod_{g=1}^p \text{N}(A_{ga}; 0, \rho_a^2) \cdot \text{Inverse-Gamma}(\rho_a^2; c_1, d_1)$$

$$= \text{Inverse-Gamma}(c_1 + \frac{p}{2}, d_1 + \frac{1}{2} \sum_{g=1}^p A_{ga}^2)$$

- Full conditional for σ_g^2 , $g = 1, \dots, p$

$$f(\sigma_g^2 | -) \propto \prod_{i=1}^n \text{N}(\mu_{ig}; \mu_g, \sigma_g^2) \cdot \text{Inverse-Gamma}(\sigma_g^2; c_2, d_2)$$

$$= \text{Inverse-Gamma}(c_2 + \frac{1}{2}n, d_2 + \frac{1}{2} \sum_{i=1}^n (\mu_{ig} - \mu_g)^2)$$

- Full conditional for ϕ_g^2 , $g = 1, \dots, p$

$$f(\phi_g^2 | -) \propto \prod_{i=1}^n \text{MVN}(\mathbf{x}_{ig}; \boldsymbol{\mu}_{ig} + (\mathbf{A}_g \circ \mathbf{Z}_g) \mathbf{Y}_i, \text{diag}(\phi_g^2, q_i)) \cdot \text{Inverse-Gamma}(\phi_g^2; c_3, d_3)$$

$$= \text{Inverse-Gamma}(c_3 + \frac{1}{2} \sum_{i=1}^n q_i, d_3 + \frac{1}{2} \sum_{i=1}^n \|\mathbf{x}_{ig} - \boldsymbol{\mu}_{ig} - (\mathbf{A}_g \circ \mathbf{Z}_g) \mathbf{Y}_i\|^2)$$

- Full conditional for predictions of gene expression (only implemented when assessing models' prediction performance on the test dataset)

Suppose that $\mathbf{X}_i^{\text{new}}, \mathbf{Y}_i^{\text{new}}$ represent predicted gene expression and factor expression of the i th individual at new time points, respectively. The posterior predictive distribution under MCEM-

algorithm-returned $\hat{\Theta}^{\text{MLE}}$ can be expressed as

$$\begin{aligned} f(\mathbf{X}_i^{\text{new}} | \hat{\Theta}^{\text{MLE}}, \Omega) &= \int f(\mathbf{X}_i^{\text{new}}, \mathbf{Y}_i^{\text{new}} | \hat{\Theta}^{\text{MLE}}, \Omega) d\mathbf{Y}_i^{\text{new}} \\ &= \int f(\mathbf{X}_i^{\text{new}} | \mathbf{Y}_i^{\text{new}}, \Omega) \cdot f(\mathbf{Y}_i^{\text{new}} | \hat{\Theta}^{\text{MLE}}, \mathbf{Y}_{i,\text{obs}}) d\mathbf{Y}_i^{\text{new}}, \end{aligned}$$

where the first term of the integrand is a MVN because of the assumed factor model, and the second term is also a MVN because of the assumed DGP model on latent factor trajectories (Shi and Choi, 2011). Therefore, once a sample of parameters Ω^r is generated, the r th sample of $\mathbf{Y}_i^{\text{new}}$ can be generated from $f(\mathbf{Y}_i^{\text{new}} | \hat{\Theta}^{\text{MLE}}, \mathbf{Y}_{i,\text{obs}}^r)$, then the r th sample of $\mathbf{X}_i^{\text{new}}$ can be sampled from $f(\mathbf{X}_i^{\text{new}} | \mathbf{Y}_i^{\text{new}}, \Omega^r)$.

A.2. Kernel Convolution Framework to Model Dependent Gaussian Processes

A.2.1. Illustration Using Two Processes

The KCF constructs correlated processes by introducing common “base processes”. Take two processes $y_a(t)$ and $y_b(t)$ as an example. KCF constructs them as,

$$\begin{aligned} y_a(t) &= \eta_a(t) + \xi_a(t) + \epsilon_a(t), \\ y_b(t) &= \eta_b(t) + \xi_b(t) + \epsilon_b(t), \end{aligned}$$

where $\epsilon_a(t)$, $\epsilon_b(t)$ are residual errors from $N(0, \psi^2)$, and $\eta_a(t)$, $\eta_b(t)$, $\xi_a(t)$, $\xi_b(t)$ are processes constructed in the following way, illustrated in Supplementary Figure 1 below.

First, three independent, zero-mean base processes $\tau_0(t)$, $\tau_a(t)$ and $\tau_b(t)$ are introduced, which are all Gaussian white noise processes. The first process $\tau_0(t)$ is shared by both $y_a(t)$ and $y_b(t)$, thereby inducing dependence between them. Whereas $\tau_a(t)$ and $\tau_b(t)$ are specific to $y_a(t)$ and $y_b(t)$, respectively; they are responsible for capturing the unique aspects of each process.

Second, Gaussian kernel functions $h_{a0}(t)$, $h_{a1}(t)$, $h_{b0}(t)$, $h_{b1}(t)$ are applied to convolve the base processes: with $h_{-0}(t)$ applied to the shared process $\tau_0(t)$ and $h_{-1}(t)$ to the output-specific processes $\tau_a(t)$ and $\tau_b(t)$,

$$\begin{aligned} \xi_a(t) &= h_{a0}(t) * \tau_0(t), & \eta_a(t) &= h_{a1}(t) * \tau_a(t), \\ \xi_b(t) &= h_{b0}(t) * \tau_0(t), & \eta_b(t) &= h_{b1}(t) * \tau_b(t), \end{aligned}$$

where the convolution operator $*$ is defined as $h(t) * \tau(t) = \int_{-\infty}^{\infty} h(t-s)\tau(s)ds$. All kernel functions $h(t)$ take the form $h(t) = v \exp\{-\frac{1}{2}Bt^2\}$, where v and B are positive parameters that are specific to

each kernel function.

A.2.2. Specific Form of Covariance Function

Under the kernel convolution framework, the covariance function between the time t_j and t_ℓ within a single process a , denoted as $C_{aa}^Y(t_j, t_\ell)$, can be decomposed as,

$$\begin{aligned} C_{aa}^Y(t_j, t_\ell) &= C_{aa}^\xi(t_j, t_\ell) + C_{aa}^\eta(t_j, t_\ell) + \delta_{j\ell}\psi^2, \\ C_{aa}^\xi(t_j, t_\ell) &= v_{a0}^2 \frac{(\pi)^{\frac{1}{2}}}{\sqrt{|B_{a0}|}} \exp\left\{-\frac{1}{4}B_{a0}d_t^2\right\}, \\ C_{aa}^\eta(t_j, t_\ell) &= v_{a1}^2 \frac{(\pi)^{\frac{1}{2}}}{\sqrt{|B_{a1}|}} \exp\left\{-\frac{1}{4}B_{a1}d_t^2\right\}, \end{aligned}$$

where j, ℓ are time indexes, $d_t = t_j - t_\ell$, and $\delta_{j\ell} = 1$ if $j = \ell$, otherwise $\delta_{j\ell} = 0$.

The covariance function between the time t_j of process a and t_ℓ of process b , denoted as $C_{ab}^Y(t_j, t_\ell)$, can be expressed as,

$$\begin{aligned} C_{ab}^Y(t_j, t_\ell) &= C_{ab}^\xi(t_j, t_\ell), \quad a \neq b, \\ C_{ab}^\xi(t_j, t_\ell) &= v_{a0}v_{b0} \frac{(2\pi)^{\frac{1}{2}}}{\sqrt{|B_{a0} + B_{b0}|}} \exp\left\{-\frac{1}{2}B_{ab}d_t^2\right\}, \end{aligned}$$

where $B_{ab} = \frac{B_{a0}B_{b0}}{B_{a0} + B_{b0}}$.

Note that the original paper (Boyle and Frean, 2005b) provides derivation results under more generalized cases. Let Q denote the dimension of the input variable t_j , and M the number of shared base process $\tau_0(t)$. In our proposed approach, $Q = 1$ and $M = 1$. In Boyle and Frean (2005b), Q, M can be arbitrary positive integers.

A.3. Choosing the Gibbs Sample Size within the MCEM Algorithm

A.3.1. Literature Review

A thorough review of strategies for choosing R can be found in Levine and Fan (2004). We focus on approaches that automatically adjust the sample size to avoid tedious manual tuning; Neath (2013) provided a review of this class of approaches. Briefly, there are primarily two methods with the main difference between them being the criterion to increase the sample size. The first approach (Booth and Hobert, 1999; Levine and Casella, 2001; Levine and Fan, 2004) achieves automatic tuning by monitoring the Monte Carlo error associated with each individual parameter, which is the approximation error incurred when using Monte Carlo samples to approximate the exact expectation. Additional samples are needed if the Monte Carlo error for any of the parameters is deemed too large. However,

this approach may be difficult to implement here because our experiments with GPFDA revealed that individual DGP parameters are not identifiable: for the same input data, different runs of GPFDA could return differing individual estimates yet still ensure similar estimates of the covariance matrix (therefore similar marginal likelihoods).

An alternative, proposed by Caffo et al. (2005), considers increasing the sample size dependent on whether the ascent property of the marginal likelihood under EM is preserved or not (Wu, 1983). For exact EM, where the expectation can be calculated precisely, the likelihood function is non-decreasing as the algorithm progresses. However, under MCEM, where the E-step is estimated with Monte Carlo samples, it is possible for the likelihood to decrease, due to approximation error. The algorithm by Caffo et al. (2005) ensures that the likelihood still increases with a high probability, as the algorithm iterates, by introducing a mechanism for rejection of proposed parameter estimates. Specifically, they use the Q-function as a proxy for the marginal likelihood. An updated $\hat{\Theta}^{(l)}$ will be accepted only when it increases the Q-function compared to the previous $\hat{\Theta}^{(l-1)}$; otherwise, the algorithm will increase the sample size and will propose a new $\hat{\Theta}^{(l)}$ using the larger sample.

A.3.2. Adaptation of Caffo's Approach to Our Model

To apply the method of Caffo et al. (2005) to our model, we begin by writing out the exact Q-function after the $(l - 1)$ th iteration of EM. Following Equations 3.5 and 3.8 of the main manuscript, $Q(\Theta, \hat{\Theta}^{(l-1)}) = \mathbb{E}_{\mathbf{Y}} \left[\ln f(\mathbf{Y}|\Theta) \middle| \mathbf{X}, \hat{\Theta}^{(l-1)} \right]$. Thus, the change in the value of the Q-function after obtaining an updated $\hat{\Theta}^{(l)}$ compared to the current $\hat{\Theta}^{(l-1)}$ can be represented as,

$$\begin{aligned} \Delta Q &= Q(\hat{\Theta}^{(l)}, \hat{\Theta}^{(l-1)}) - Q(\hat{\Theta}^{(l-1)}, \hat{\Theta}^{(l-1)}) \\ &= \mathbb{E}_{\mathbf{Y}} \left[\ln \frac{f(\mathbf{Y}|\hat{\Theta}^{(l)})}{f(\mathbf{Y}|\hat{\Theta}^{(l-1)})} \middle| \mathbf{X}, \hat{\Theta}^{(l-1)} \right] \\ &= \mathbb{E}_{\mathbf{Y}} [g(\mathbf{Y})], \end{aligned}$$

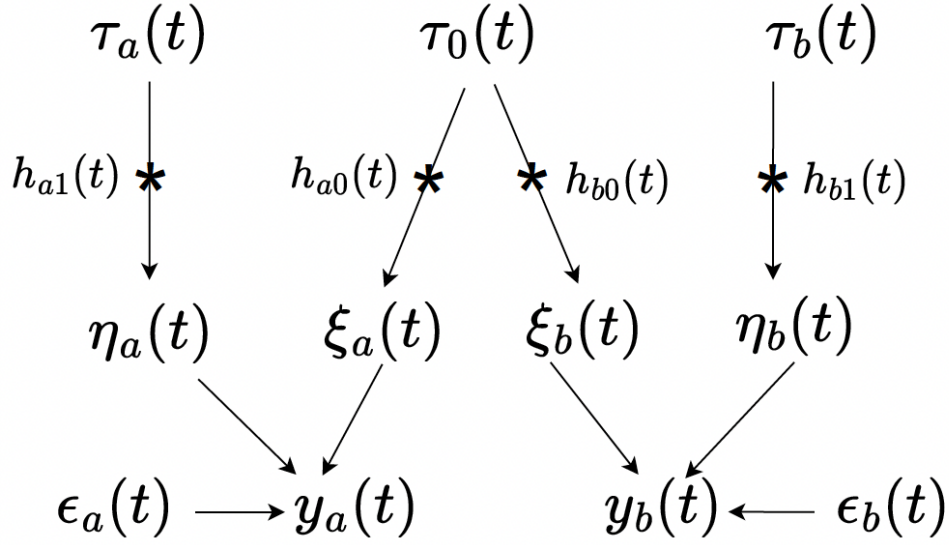
where $g(\mathbf{Y}) = \ln \frac{f(\mathbf{Y}|\hat{\Theta}^{(l)})}{f(\mathbf{Y}|\hat{\Theta}^{(l-1)})}$, and the expectation is with respect to $f(\mathbf{Y}|\mathbf{X}, \hat{\Theta}^{(l-1)})$. Under MCEM, we approximate this change ΔQ using the approximate Q-function \tilde{Q} in Equation 3.7,

$$\begin{aligned}\Delta\tilde{Q} &= \tilde{Q}(\hat{\Theta}^{(l)}, \hat{\Theta}^{(l-1)}) - \tilde{Q}(\hat{\Theta}^{(l-1)}, \hat{\Theta}^{(l-1)}) \\ &= \frac{1}{R} \sum_{r=1}^R \ln \frac{f(\mathbf{Y}^r|\hat{\Theta}^{(l)})}{f(\mathbf{Y}^r|\hat{\Theta}^{(l-1)})} \\ &= \frac{1}{R} \sum_{r=1}^R g(\mathbf{Y}^r), \quad \mathbf{Y}^r \sim f(\mathbf{Y}|\mathbf{X}, \hat{\Theta}^{(l-1)}) \\ &= \bar{g}_R.\end{aligned}$$

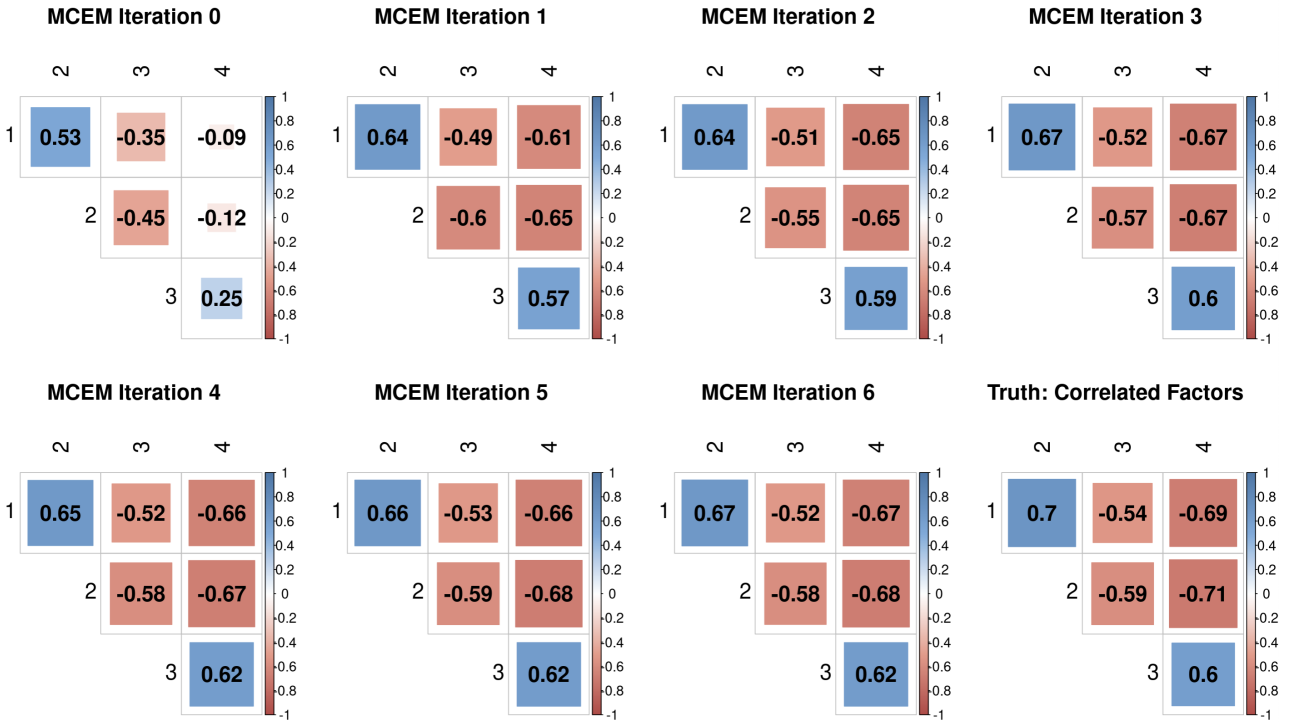
A generalized version of the Central Limit Theorem (CLT) (Jones, 2004) shows that \bar{g}_R converges, in distribution, to $N(\mathbb{E}_{\mathbf{Y}}[g(\mathbf{Y})], \frac{\zeta}{R})$ as $R \rightarrow \infty$, where $\zeta = \text{Var}(g(\mathbf{Y}))$ can be estimated using either the sample variance of $g(\mathbf{Y}^r)$ when the samples $\{\mathbf{Y}^r\}_{r=1,\dots,R}$ are independent, or the batch means approach (Lunn et al., 2013; Guan and Haran, 2019) when the samples are dependent (as is the case here, because they are obtained using an MCMC sampler). This implies that,

$$\begin{aligned}P\left(\frac{\bar{g}_R - \mathbb{E}_{\mathbf{Y}}[g(\mathbf{Y})]}{\sqrt{\frac{\hat{\zeta}}{R}}} < Z_{1-\alpha}\right) &\approx 1 - \alpha; \text{ or equivalently,} \\ P\left(\Delta Q > \Delta\tilde{Q} - \sqrt{\frac{\hat{\zeta}}{R}} Z_{1-\alpha}\right) &\approx 1 - \alpha,\end{aligned}$$

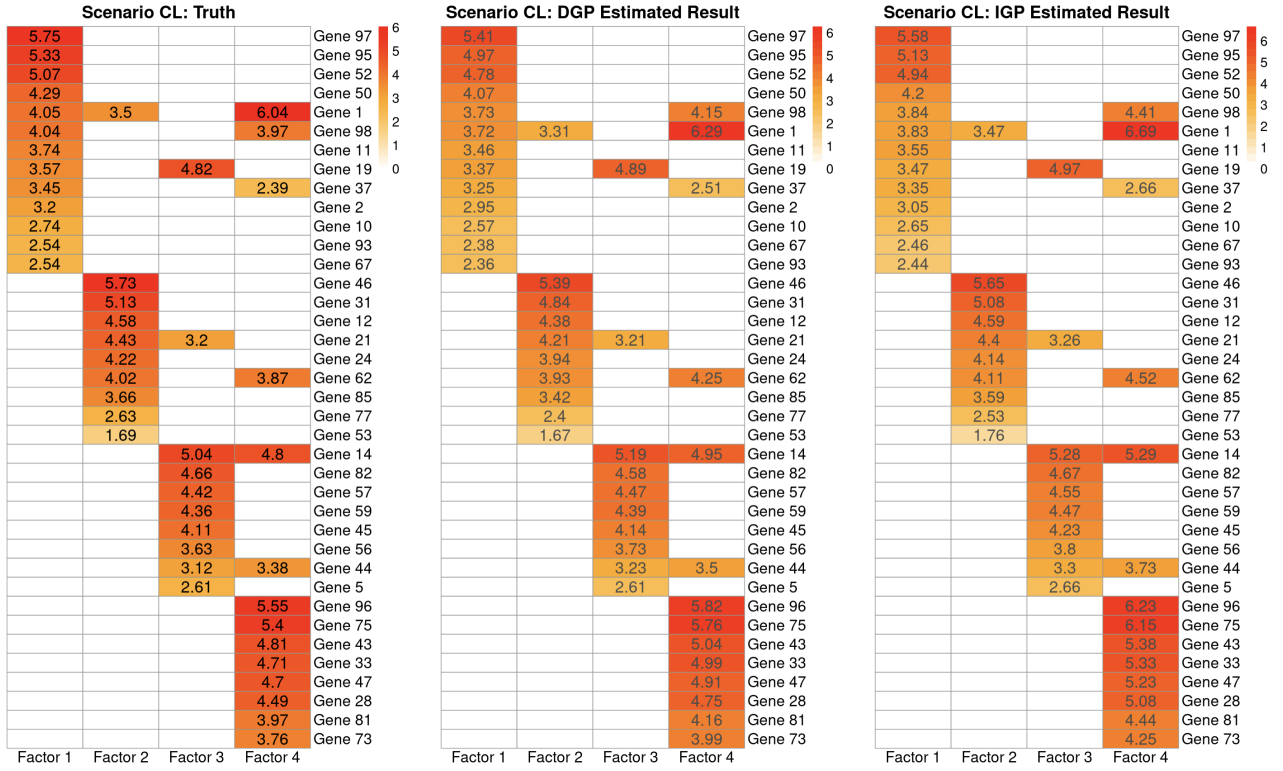
where $\hat{\zeta}$ is the estimate of ζ , $Z_{1-\alpha}$ is the upper α quantile of the standard normal distribution. $(\Delta\tilde{Q} - \sqrt{\frac{\hat{\zeta}}{R}} Z_{1-\alpha})$ is called the “Lower Bound” (LB) for ΔQ (Caffo et al., 2005) because there is a high chance that ΔQ is larger than this estimator if we choose α to be small. When LB is positive, it is highly likely that ΔQ is also positive. The automatic updating rule for the sample size is based on LB. In the l th iteration, if LB is positive, then we accept the updated $\hat{\Theta}^{(l)}$ and keep the current sample size R ; otherwise, we reject $\hat{\Theta}^{(l)}$ and continue generating additional samples under $\hat{\Theta}^{(l-1)}$ for updating again. Caffo et al. (2005) suggests a geometric rate of increase for the sample size, by drawing additional $\frac{R}{m}$ samples for some fixed m .



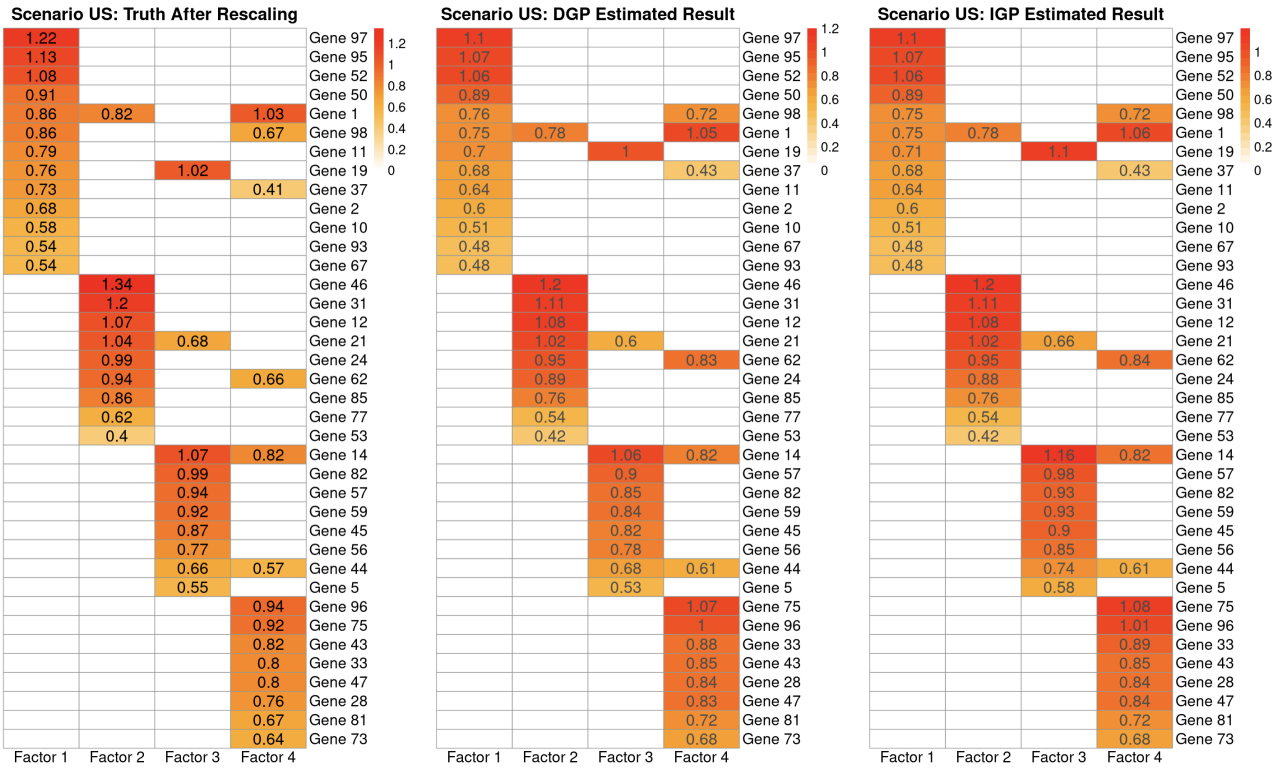
Supplementary Figure 1: Illustration of the kernel convolution framework for DGPs. The star (*) denotes a convolutional operation and directed arrows indicate direct dependence. t denotes time; a, b are indexes of factor trajectories; $\tau_a(t), \tau_0(t), \tau_b(t)$ are independent Gaussian white noise processes; $h_{a1}(t), h_{a0}(t), h_{b0}(t), h_{b1}(t)$ are Gaussian kernel functions; $\epsilon_a(t), \epsilon_b(t)$ are residuals; $y_a(t), y_b(t)$ are the a th and b th factor trajectories, respectively.



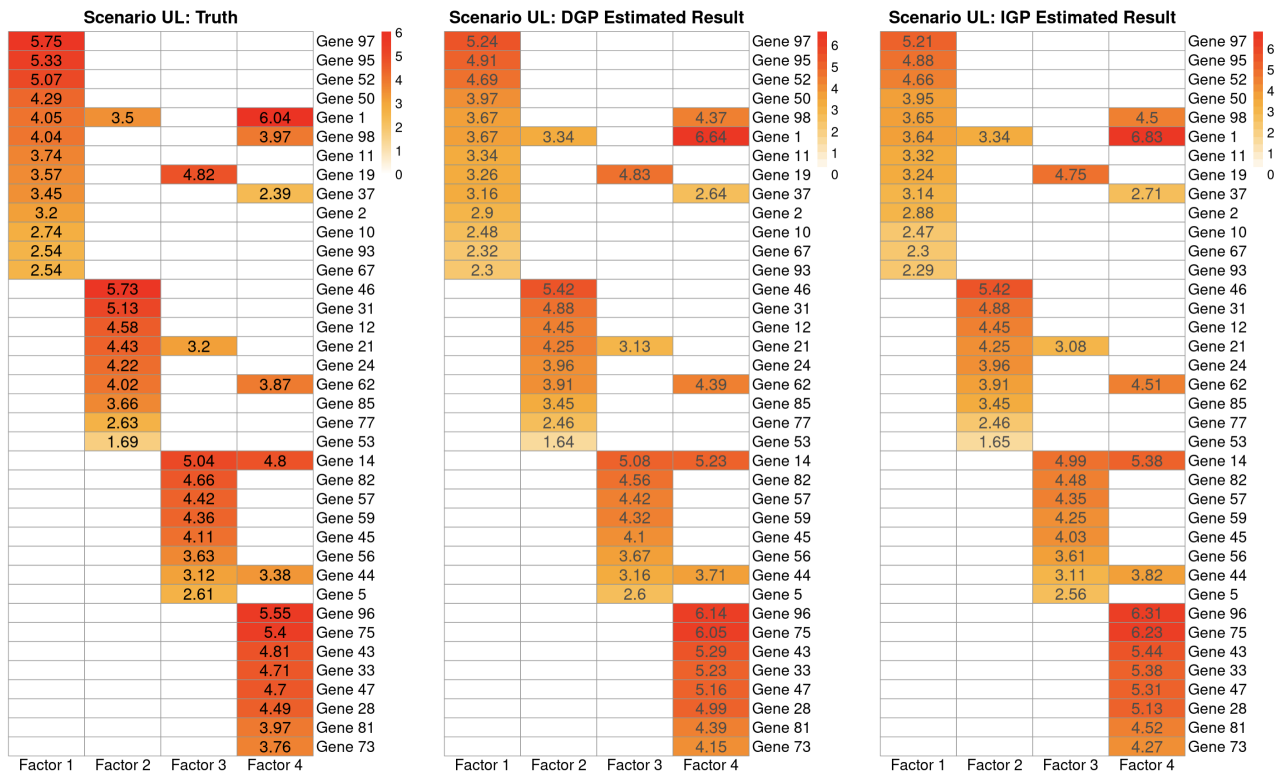
Supplementary Figure 2: An example of cross-correlation matrices at MCEM iterations 0 (initial value) to 6 during the MCEM algorithm using the DGP model: scenario CS, number of latent factors k correctly specified as 4. The true cross-correlation matrix is also shown.



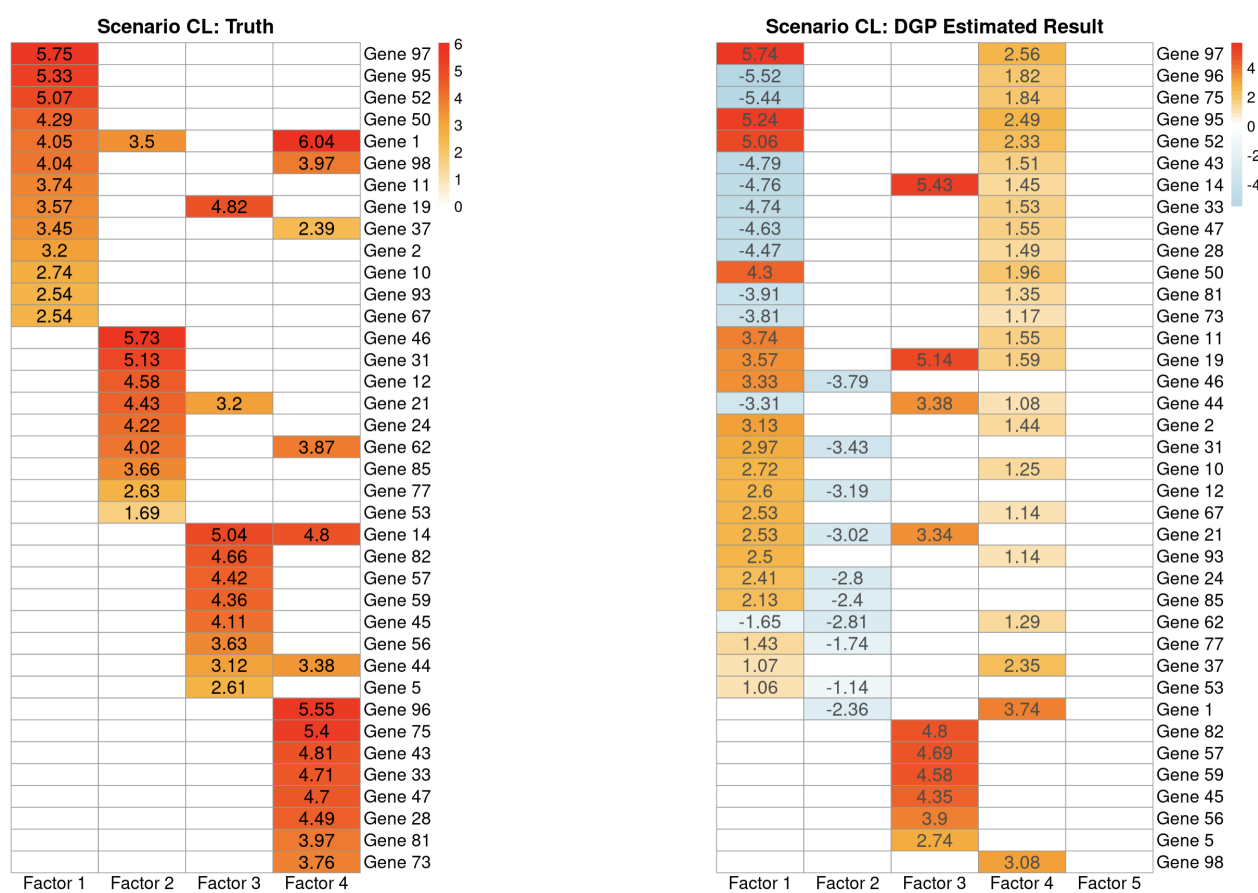
Supplementary Figure 3: Comparison between true and estimated factor loadings: scenario CL, number of latent factors k correctly specified as 4. Genes displayed in each heatmap are ordered following the same two rules: first, genes on factors with smaller indexes are ranked first; second, genes with larger absolute factor loadings are ranked first.



Supplementary Figure 4: Comparison between true and estimated factor loadings: scenario US, number of latent factors k correctly specified as 4. Genes displayed in each heatmap are ordered following the same two rules: first, genes on factors with smaller indexes are ranked first; second, genes with larger absolute factor loadings are ranked first.



Supplementary Figure 5: Comparison between true and estimated factor loadings: scenario UL, number of latent factors k correctly specified as 4. Genes displayed in each heatmap are ordered following the same two rules: first, genes on factors with smaller indexes are ranked first; second, genes with larger absolute factor loadings are ranked first.



Supplementary Figure 6: Comparison between true and estimated factor loadings using the DGP model: scenario CL, with the number of latent factors k mis-specified as 5. Genes displayed in each heatmap are ordered following the same two rules: first, genes on factors with smaller indexes are ranked first; second, genes with larger absolute factor loadings are ranked first.

13 chart records [Download File](#)

Sublist	Category	Term	RT	Genes	Count	%	P-Value	Benjamini
<input type="checkbox"/>	KEGG_PATHWAY	Coronavirus disease - COVID-19	RT	<div></div>	11	22.0	1.6E-9	7.5E-8
<input type="checkbox"/>	KEGG_PATHWAY	Influenza A	RT	<div></div>	10	20.0	7.9E-9	1.9E-7
<input type="checkbox"/>	KEGG_PATHWAY	Hepatitis C	RT	<div></div>	9	18.0	7.9E-8	1.2E-6
<input type="checkbox"/>	KEGG_PATHWAY	RIG-I-like receptor signaling pathway	RT	<div></div>	6	12.0	5.3E-6	6.2E-5
<input type="checkbox"/>	KEGG_PATHWAY	Measles	RT	<div></div>	7	14.0	1.6E-5	1.5E-4
<input type="checkbox"/>	KEGG_PATHWAY	Epstein-Barr virus infection	RT	<div></div>	7	14.0	1.3E-4	9.9E-4
<input type="checkbox"/>	KEGG_PATHWAY	NOD-like receptor signaling pathway	RT	<div></div>	6	12.0	3.1E-4	2.1E-3
<input type="checkbox"/>	KEGG_PATHWAY	Herpes simplex virus 1 infection	RT	<div></div>	7	14.0	1.1E-3	6.5E-3
<input type="checkbox"/>	KEGG_PATHWAY	Cytosolic DNA-sensing pathway	RT	<div></div>	4	8.0	1.2E-3	6.5E-3
<input type="checkbox"/>	KEGG_PATHWAY	Pertussis	RT	<div></div>	3	6.0	3.5E-2	1.6E-1
<input type="checkbox"/>	KEGG_PATHWAY	Complement and coagulation cascades	RT	<div></div>	3	6.0	4.5E-2	1.9E-1
<input type="checkbox"/>	KEGG_PATHWAY	Viral protein interaction with cytokine and cytokine receptor	RT	<div></div>	3	6.0	5.6E-2	2.2E-1
<input type="checkbox"/>	KEGG_PATHWAY	Chagas disease	RT	<div></div>	3	6.0	6.6E-2	2.4E-1

Supplementary Figure 7: Results under the KEGG Pathway analysis of the online bioinformatics platform DAVID.

Supplementary Algorithm 1: Gibbs-after-MCEM Algorithm for Posterior Summary.

Input :

- Observed gene expression \mathbf{X}_i and time points \mathbf{t}_i , $i = 1, \dots, n$ for n people.
- Prediction time points \mathbf{t}^{new} .
- $\hat{\Theta}^{\text{MLE}}$.
- Number of parallel chains C .

Output:

- Posterior samples of Ω , including the pathway expression \mathbf{Y}_i , $i = 1, \dots, n$ and gene-pathway relationship \mathbf{L} .
- Posterior samples of predicted gene expression $\mathbf{X}_i^{\text{new}}$, $i = 1, \dots, n$ at \mathbf{t}^{new} .

1 Step 1: Initialization Step

- Construct $\hat{\Sigma}_{\mathbf{Y}}^{\text{MLE}}$ using $\hat{\Theta}^{\text{MLE}}$, $\mathbf{t} = \bigcup_{i=1}^n \mathbf{t}_i$ and \mathbf{t}^{new} .
- Specify the Gibbs sample size R^{final} .

Step 2: Sample Generation Step

Run C chains in parallel, and under each chain: draw R^{final} samples of Ω using the Gibbs sampler $f(\Omega|\mathbf{X}, \hat{\Sigma}_{\mathbf{Y}}^{\text{MLE}})$, then $\mathbf{X}_i^{\text{new}}$ from $f(\mathbf{X}_i^{\text{new}}|\Omega, \hat{\Sigma}_{\mathbf{Y}}^{\text{MLE}})$. Post-process samples by burn-in and thinning, and denote the remaining sample size as $R_{\text{remain}}^{\text{final}}$.

Step 3: Sample Alignment Step

Align post-processed samples $\{\mathbf{L}^r, \mathbf{Y}_i^r\}_{r=1, \dots, R_{\text{remain}}^{\text{final}}}$ within each chain, then across chains; both can be achieved using R package “factor.switch”.

Supplementary Table 1: Max Rhat for each type of key variables: all scenarios, number of latent factors k correctly specified as 4. MCMC iteration number was increased to 100,000 if Rhat under 10,000 iterations suggested non-convergence.

Scenario US		
Model Variable	DGP MCMC iteration = 10,000	IGP MCMC iteration = 10,000
Predicted gene expression	1.01	1.01
Factor loadings	1.02	1.02
Latent factors	1.01	1.01
Scenario CS		
Model Variable	DGP MCMC iteration = 10,000	IGP MCMC iteration = 100,000 (10,000)
Predicted gene expression	1.01	1.04 (1.02)
Factor loadings	1.01	1.09 (4.37)
Latent factors	1.01	1.04 (2.45)
Scenario UL		
Model Variable	DGP MCMC iteration = 100,000 (10,000)	IGP MCMC iteration = 100,000 (10,000)
Predicted gene expression	1.04 (1.01)	1.04 (1.01)
Factor loadings	1.04 (1.48)	1.06 (1.48)
Latent factors	1.05 (1.40)	1.06 (1.40)
Scenario CL		
Model Variable	DGP MCMC iteration = 100,000 (10,000)	IGP MCMC iteration = 100,000 (10,000)
Predicted gene expression	1.04 (1.01)	1.04 (1.01)
Factor loadings	1.02 (1.29)	1.06 (1.45)
Latent factors	1.04 (1.25)	1.06 (1.37)

Supplementary Table 2: Prediction results for all scenarios: number of latent factors k mis-specified as 3 or 5 for the DGP model. $MAE_{\mathbf{X}}$, $MWI_{\mathbf{X}}$ and $PWI_{\mathbf{X}}$ are short for mean absolute error, mean width of the 95% predictive intervals, and the proportion of genes within 95% the predictive intervals, respectively.

Factor Generation Mechanism		DGP, $k = 3$			DGP, $k = 5$		
Correlation	Variability	$MAE_{\mathbf{X}}$	$MWI_{\mathbf{X}}$	$PWI_{\mathbf{X}}$	$MAE_{\mathbf{X}}$	$MWI_{\mathbf{X}}$	$PWI_{\mathbf{X}}$
Correlated	Large	1.30	6.63	0.95	1.34	6.83	0.95
	Small	0.55	2.77	0.95	0.54	2.74	0.95
Uncorrelated	Large	1.40	7.26	0.95	1.51	7.70	0.95
	Small	0.56	2.94	0.95	0.56	2.81	0.95

Supplementary Table 3: Top 50 genes sorted according to absolute factor loadings. Numbers within the parenthesis in the right column represent rank of this gene in the left column, and “-” denote this gene is not in the left column. Note that names beginning with “M97935” in Chen et al. (2011) are actually control sequences rather than genes.

Row Index	Principal Factor by Chen et al. (2011)	Factor 1 by Our Approach
1	RSAD2	LAMP3 (13)
2	IFI44L	RSAD2 (1)
3	IFIT1	IFI44L (2)
4	IFI44	SERPING1 (10)
5	HERC5	SPATS2L (-)
6	OAS3	SIGLEC1 (22)
7	MX1	ISG15 (8)
8	ISG15	IFIT1 (3)
9	IFIT3	IFI44 (4)
10	SERPING1	RTP4 (35)
11	IFIT2	OAS3 (6)
12	OASL	IFI6 (17)
13	LAMP3	CCL2 (-)
14	IFI27	IDO1 (-)
15	OAS1	HERC5 (5)
16	OAS2	MS4A4A (-)
17	IFI6	IFIT3 (9)
18	IFIT5	OAS1 (15)
19	IFITM3	OAS2 (16)
20	XAF1	LY6E (24)
21	DDX58	OASL (12)
22	SIGLEC1	ATF3 (-)
23	DDX60	CXCL10 (-)
24	LY6E	CCL8 (-)
25	GBP1	XAF1 (20)
26	IFIH1	IFI27 (14)
26	LOC26010	SAMD4A (-)
28	ZCCHC2	MX1 (7)
29	EIF2AK2	LGALS3BP (-)

30	LAP3	C1QB (-)
31	IFI35	IFITM3 (19)
32	IRF7	LAP3 (30)
33	PLSCR1	IRF7 (32)
34	M97935_MA_at	ZBP1 (42)
35	RTP4	HERC6 (37)
36	M97935_MB_at	TFEC (-)
37	HERC6	IFI35 (31)
38	TNFAIP6	MT2A (-)
39	PARP12	SCO2 (41)
40	M97935_5_at	DDX58 (21)
41	SCO2	IFIH1 (26)
42	ZBP1	IFIT2 (11)
43	STAT1	DHX58 (-)
44	UBE2L6	TMEM255A (-)
45	MX2	TNFAIP6 (38)
46	TOR1B	VAMP5 (-)
47	M97935_3_at	PARP12 (39)
48	TNFSF10	GBP1 (25)
49	TRIM22	TIMM10 (-)
50	APOL6	C1QA (-)